Original research article

Journal of Neuromuscular Diseases
1–24

DOI: 10.1177/22143602251409302
journals.sagepub.com/home/jnd

Sage | IOS Press

Identification of myokines associated with the pathological stress response in the *mdx* mouse model of Duchenne muscular dystrophy

Erynn E Johnson[1], Jacob Powers[1] and James M Ervasti[1]

Abstract

Purpose: Skeletal muscle constitutes 30–40% of total body mass and is now considered an endocrine organ, given its secretion of a variety proteins, metabolites, and cytokines. We have previously shown that the absence of dystrophin in skeletal muscle contributes to lethal systemic stress pathology in the *mdx* mouse model of Duchenne muscular dystrophy through a mechanism that remains to be identified. Here we searched for secreted protein signaling factors, or myokines, released from dystrophin-deficient skeletal muscle that influence the organism-wide integrated stress response. We performed skeletal muscle extracellular fluid extraction and discovery proteomics for wild-type, *mdx*, and transgenic *mdx* mice rescued by expression of a dystrophin construct, all analyzed under basal conditions and following brief scruff restraint stress that causes inactivity in *mdx* mice.

Major Findings: Our analysis demonstrated that skeletal muscle dystrophinopathy is associated with increased expression of numerous proteins in both intact *mdx* skeletal muscle and extracellular fluid compared to healthy mice. Brief scruff restraint revealed protein candidates with differential abundance in *mdx* extracellular fluid. Specifically, altered follistatin-like 1 protein and adiponectin secretion in response to scruff stress was shown to be dependent on skeletal muscle dystrophinopathy. The diverse signaling roles of follistatin-like 1 in the cardiovascular, musculoskeletal, and nervous system implicate it as a particularly intriguing myokine candidate regulating the *mdx* stress response.

Conclusions: Our current study informs on the skeletal muscle secretory profile in *mdx* following a stressful stimulus and provides new leads to elucidate the mechanism by which *mdx* skeletal muscle orchestrates inter-organ stress signaling.

Keywords

duchenne muscular dystrophy, skeletal muscle, myokine, stress physiology, proteomics

Received: 2 September 2025; accepted: 4 December 2025

Background

Duchenne muscular dystrophy (DMD) is a progressive fatal neuromuscular disease characterized by loss-of-function mutations in the *DMD* gene that lead to a loss of dystrophin protein. Primary defects associated with the loss of dystrophin in skeletal, cardiac, and smooth muscle include progressive muscle degeneration and weakness, which are associated with chronic inflammation, muscle necrosis and fibrosis, respiratory distress, and cardiomyopathy.[1] DMD patients also suffer from secondary effects of dystrophinopathy in muscle and non-muscle tissues, with disease comorbidities including neurocognitive and behavioral challenges,[2–4] heightened stress sensitivity,[5] scoliosis,[1] and metabolic dysfunction.[4,6,7] Importantly, we have shown that the *mdx* mouse model of DMD exhibits dramatic stress pathology, with mild scruff stress provoking tonic immobility and transient hypotension, and more severe social defeat stress triggering sustained immobility, hypotension, and lethality.[8,9] The MTBD/*mdx* mouse line transgenically restores dystrophin exclusively in the skeletal muscle (SkM) and rescues *mdx* stress pathology along with hallmark defects in *mdx* SkM morphology and

[1]Department of Biochemistry, Molecular Biology, and Biophysics, University of Minnesota Medical School, Minneapolis, MN, 55455, USA

Corresponding author:
Dr James M Ervasti, Professor, University of Minnesota, Research Director, Greg Marzolf Jr. Muscular Dystrophy Center
Email: jervasti@umn.edu

force generation capacity.[8,10] The pathological consequences of SkM dystrophinopathy highlight the centrality of SkM, which constitutes 30–40% of total body mass and serves as a primary hub for protein metabolism,[11] in regulating organismal health. While we have previously sought to identify how SkM metabolism influences systemic stress responses in *mdx* mice,[9] our current study investigates the role of SkM-secreted cytokines, peptides, and proteins – known as myokines – in regulating stress behavior in the context of healthy and dystrophin-deficient SkM.

Beyond its role in force production and locomotion, SkM is also an important endocrine organ.[12] The SkM secretome, comprised of myokines, nucleotides, and myometabolites released primarily during muscle contraction, has been shown to mediate inter-organ signaling crosstalk and participates in various organism-wide cellular and immune processes[12–15]. Given the systemic pathological consequences of SkM dystrophin deficiency,[8,10] it is of great interest to identify altered patterns of myokine secretion in *mdx* SkM that regulate inter-organ crosstalk and central stress circuitry, as well as to observe how transgenic restoration of dystrophin in MTBD/*mdx* mice restores myokine and stress circuitry defects to protect against stress pathology. However, there are several experimental limitations to studying myokines within the SkM secretome, including the dynamic range problem of plasma or serum proteomics that masks detection of low-abundance molecules,[16] analogous signal dilution issues stemming from bulk tissue analysis,[17] and the need to unequivocally identify the tissue origin of an analyte within a broader circulating pool of molecules secreted from various organs. While exosome and extracellular vesicle isolation methods that allow for myokine detection have grown in popularity and sophistication over the years, they remain limited by reproducibility issues and the possible exclusion of myokines released through non-canonical secretion pathways.[18,19]

Recent work by the Chouchani and Spiegelman laboratories established a novel and simplified approach to isolate inter-myocyte extracellular fluid (ECF) from SkM for the proteomic characterization of myokines whose low abundance and extracellular localization preclude detection in a crude whole-tissue extract.[17,20] Combining a SkM ECF and bulk SkM tissue proteomics analysis using the same muscle samples holds the unique advantage of being able to identify proteins that are actively secreted from SkM in response to an intervention. In this study, we utilized an ECF isolation and isobaric labeling discovery proteomics strategy with the goal of capturing stress-regulatory myokines at their site of secretion from quadriceps SkM in wild-type (WT), *mdx*, and MTBD/*mdx* mice at baseline and after mild scruff exposure that provokes *mdx* stress pathology.[8,9] Herein, we demonstrate that *mdx* mice exhibit distinct ECF and bulk quadriceps muscle (QM) proteomic landscapes compared with WT or MTBD/*mdx* mice at baseline and after scruff stress. We show that *mdx* proteomic shifts are largely returned to WT levels in MTBD/*mdx* skeletal muscle, confirming a rescue of proteomic dysfunction in dystrophin-replete MTBD/*mdx* SkM and ECF that parallels a correction in stress pathology in the MTBD/*mdx* mouse. We mined our proteomics data for proteins with differential expression after scruff stress in the *mdx* ECF compartment compared to WT that are rescued in MTBD/*mdx* mice and identified follistatin-like 1 (FSTL1) protein as one interesting lead that matched the desired characteristics of altered expression in the *mdx* ECF compartment corresponding to stress. Elevated FSTL1 has been implicated in pathological adaptations to chronic stress exposure as well as inflammatory diseases while also demonstrating protective and regenerative cardiovascular capacities,[21–23] suggesting its potential relevance to *mdx* stress pathology.

Methods

Mice

The mice used in this study were adult males (3–4 months of age). Animal care and experimental procedures were approved by the Institutional Animal Care and Use Committee (IACUC) of the University of Minnesota. C57BL6/J and C57BL10/J mice used as wild-type controls and C57BL/10ScSn-*Dmd*^{mdx}/J (*mdx*) mice were bred in-house or purchased from The Jackson Laboratory. The previously described MTBD/*mdx* transgenic mouse line[10] expressing a human skeletal actin promotor-driven full-length dystrophin/utrophin chimera with microtubule-binding spectrin repeats 20–24 of dystrophin replaced by non-binding repeats 18–22 of utrophin was generated in our lab and bred in-house. Mice were group housed following standard specific pathogen free (SPF) procedures with *ad libitum* access to food and water on a 12-h light/dark cycle.

Scruff-induced inactivity

The scruff stress assay was implemented following an established protocol.[8,9] Briefly, mouse locomotor activity was assessed using the SuperFlex Open Field activity monitoring system and associated AccuScan Fusion software (Version 3.4) by Omnitech Electronics, Inc. Following 30 min activity monitoring, mice were scruffed by the nape of the neck using the thumb and forefinger and placing the tail between the 5th digit and palm of the hand. Immediately following 30 s scruff, mice were released into the same activity box and locomotor activity monitoring resumed for 30 min, after which mice were anesthetized with tribromoethanol (Avertin) and euthanized via cervical dislocation. Quadriceps muscle was quickly

dissected after euthanasia and processed for ECF isolation and proteomics analysis.

Quadriceps tissue harvest and extracellular fluid isolation

We adapted a recent protocol from Mittenbuhler et al.[17] to isolate ECF from mouse quadriceps muscle. Quadriceps muscles from both hind limbs were dissected, transferred to the center of a 20μm nylon mesh (Millipore Sigma, NY2004700), then the mesh was folded into a conical shape and secured in a 1.5 mL centrifuge tube. The samples were centrifuged at 800xg for 10 min at 4°C, which produced 10–20μL ECF. Isolated ECF samples from the left and right hindlimb of the same mouse were pooled, snap frozen, and stored at −80°C. The remaining ECF-depleted quadriceps muscle tissue was snap frozen and stored at −80°C for downstream processing and mass spectrometry analysis.

Immunodepletion of extracellular fluid

Quadriceps ECF samples were immunodepleted to remove high-abundance plasma and serum proteins albumin and IgG using R&D Systems Proteome Purify 2 Mouse Serum Protein Immunodepletion Resin (R&D Systems, MIDR002020). Samples (10μL) were mixed with 1 mL of immunodepletion resin and rotated end-over-end at room temperature for 1hr, then resin was split between two SpinX filter tubes (R&D Systems, SPINX8160036) and centrifuged at 1,500xg for 2 min. Eluates were collected and protein concentration was determined using A280 absorbance measurements, then samples were concentrated using Vivaspin® 500 3 kDa centrifugal concentrator tubes (Sartorius, VS0192). Concentrated samples were snap frozen and kept at −80°C for downstream processing and mass spectrometry analysis.

Western blot analysis

Quad muscle was homogenized using mortar and pestle in liquid nitrogen. Crushed tissue was lysed with 1% sodium dodecyl sulfate in 1xPBS with added protease inhibitors (100 nM Aprotonin, 10 mg/mL E-64, 100μM Leupeptin, 1 mM PMSF, 1μg/mL Pepstatin, 0.79 mg/mL Benzamidine). Lysates were clarified by centrifugation, then protein content was assessed by A_{280} absorbance and samples were diluted to 2 mg/mL with PBS and β-mercaptoethanol for protein denaturation. Forty μg total protein was loaded on a 10% polyacrylamide gel for 20 min at 80 V, then 1hr at 120 V or until dye front ran off gel. Protein was transferred to a 0.45μm polyvinylidene fluoride membrane (Immobilon-FL IPFL00010, Millipore Sigma) overnight on ice at 20 V with methanol added to transfer buffer (25 mM Tris, 192 mM glycine, 10% methanol). Membranes were blocked with 5% bovine serum albumin (BSA) in TBST for 1 h before incubation with primary antibodies for 1.5 h at room temperature. Primary antibodies were diluted in 5% BSA in TBST: anti-FSTL1 (20182-1-AP, Proteintech) at a 1:5000 dilution and anti-α-tubulin (B512, Invitrogen) at a 1:1000 dilution. Secondary antibodies DyLight 680 and 800 (1:10,000, Cell Signaling) were incubated in the dark for 1 h at room temperature. Membranes were imaged and densitometry quantifications were made with a Licor Odyssey Infrared Imaging System and Image Studio Lite (5.x CLx/DLx) software.

ELISA analysis

A commercial FSTL1 ELISA kit (CSB-EL009025MO, CusaBio, Wuhan, China) was employed as an orthogonal approach to validate proteomics results. Quad muscle, ECF, and plasma were harvested from the same mice and used for ELISA analysis. Quad muscle and ECF were also used for WB and proteomics analyses. Aliquots of ECF-depleted quadriceps lysates processed for WB analysis were diluted 1:2 and used for ELISA quantification. Immunodepleted quadriceps ECF was diluted to 0.1 mg/mL and ELISA analysis was performed following the manufacturer instructions. Briefly, 100μL aliquots of diluted quadriceps lysates, quadriceps ECF, and plasma were incubated in antibody-coated wells for 2 h at 37°C along with a serial dilution of the provided FSTL1 standard to generate a standard curve. Technical duplicates were analyzed for quad lysates, while low sample amounts precluded technical replicate analysis for ECF and plasma. Biotin-antibody conjugation to antibody-immobilized samples was performed for 1 h at 37°C, followed by three washes and incubation with HRP-avidin for 1 h at 37°C. Samples were washed for five cycles, then TMB substrate was allowed to react with HRP for 15–30 min before quenching with stop solution. Colorimetric detection was performed with a SpectraMax iD3 Multi-Mode Microplate Reader (Avantor) at 450 nm within five minutes of adding stop solution. A standard curve was generated by plotting FSTL1 concentration on the x axis and blank-corrected absorbance units on the y axis, then a linear or polynomial regression fit was used for interpolation to determine analyte FSTL1 concentration.

Protein extraction, digestion, and peptide isobaric labeling

Frozen quadricep muscle tissue pieces (20–25 mg) were processed using a Percellys Cryolys Evolution bead

beater (Bertin Technologies). Tissue samples were weighed in Percellys tissue homogenizing CKMix tubes (Bertin Technologies) and protein extraction buffer [7 M urea, 2 M thiourea, 0.4 M Tris pH 8.0, 20% (v/v) acetonitrile, 10 mM tris (2-carboxyethyl) phosphine (TCEP), 40 mM chloroacetamide, and 1µl/100ul buffer Pierce Universal Nuclease (Thermo Fisher Scientific)] was added at a ratio of 9ul lysis buffer per 1 mg tissue. A 150µl aliquot of each sample was transferred to a PCT tube with a 150µl cap for the Barocycler NEP2320 (Pressure Biosciences, Inc., South Easton, MA) and cycled between 35 kPSI for 20 s and 0 kPSI for 10 s for 60 cycles at 37°C. After barocycling, the samples were centrifuged at 15,000xg for 10 min. The samples were transferred to new 1.5 mL microfuge Eppendorf Protein LoBind tubes. Aliquots for each sample in the quadriceps muscle (QM) and ECF experiment were taken for protein concentration determination by Bradford assay.

A bridged pooled normalizing sample was made for ECF and muscle TMTpro 16plex (Tandem Mass Tag, Thermo Fisher Scientific, Waltham, MA) experiments. The pooled sample was composed of equal µg aliquots of each sample within the ECF or whole muscle experiment.

For the ECF TMTpro experiment, a 15µg aliquot of each sample and pooled sample was transferred to a new 1.5 mL Eppendorf Protein LoBind tube and brought to the same volume with PBS. A fourfold volume of extraction buffer was added to each sample and incubated at 37°C for 30 min. The extraction buffer volume was diluted fivefold with LC-MS grade water.

For the whole muscle TMTpro experiment, an 18µg aliquot of each sample and pooled sample was transferred to a new 1.5 mL Eppendorf Protein LoBind tube and brought to the same volume with extraction buffer. The samples were diluted fivefold with LC-MS grade water.

For all samples, trypsin (Promega, Madison, WI) was added in a 1:40 ratio of trypsin to total protein. Samples were incubated at 37°C overnight, then were acidified with 0.3% (v/v) formic acid. Samples were cleaned using a MCX Stage tip and eluates were vacuum dried. Samples were resuspended with 0.1 M triethylammonium bicarbonate, pH 8.5, to a final protein concentration of 1µg/µL.

For stable isotope labeling, a 14µg aliquot for each sample in the whole muscle TMTpro experiment and 12µg aliquot for each sample in the ECF TMTpro experiment was made and assigned a channel within a TMTpro 16plex. The samples were labeled with TMTpro 16plex isobaric label reagent in a 1:10 ratio of µg protein to µg TMTpro 16plex label according to the manufacturer's instructions. Isobaric tag-labeled samples within the same experimental screen were multiplexed together into a new 1.5 mL Eppendorf tube, then vacuum dried and cleaned with a 1 mL SepPak C18 solid phase extraction cartridge (Waters Corporation, Milford, MA). Each TMTpro 16plex sample was vacuum dried, resuspended in 20 mM ammonium formate, pH 10, 98% (v/v) water and 2% (v/v) acetonitrile and fractionated offline by high pH C18 reversed-phase chromatography as previously described.[24] After fractionation, concatenated peptide fractions were C18 Stage tipped[25] and eluates were dried *in vacuo*.

Mass spectrometry data acquisition

ECF and QM proteomics experiments were performed at the University of Minnesota in collaboration with the Center for Metabolomics and Proteomics (CMSP) departmental core facility. Six experimental groups of mice (3–4 months old) were tested, including WT (C57BL/10J), *mdx* (C57BL/10 ScSn-Dmd^{mdx}/J), and MTBD/*mdx* mice sacrificed at baseline or 30 min following a 30 s scruff stress exposure (n = 5 mice/group). Thirty total samples were collected and two TMTpro 16plex screens were run for each of the two biological compartments (ECF and QM) for a total of four screens, with a pooled normalization control sample included in each screen (Figure 1A). All data were collected on a Thermo Orbitrap Eclipse™ mass spectrometer coupled to a Dionex™ Ultimate™ 3000 RSLCnano LC pump. Peptides from 20% (3µL) of each concatenated set of fractions were separated using a 199-min gradient at 0.315–0.350µL/min on a C18-AQ ReproSil-Pur column measuring 300 mm with an internal diameter of 100µm, 1.9µm resin size, and 120 Å pore size (Dr Maisch GmbH Ammerbuch, Germany). Buffer A consisted of water with 0.1% (v/v) formic acid and Buffer B consisted of acetonitrile with 0.1% (v/v) formic acid. High-field asymmetric-waveform ion mobility spectroscopy (FAIMS) was enabled during experimental acquisition with the following compensation voltage (CV) settings: −45 V, −60 V, and −75 V. Voltage was kept at 2.1 kV for positive ion mode and the ion transfer tube temperature was set to 275°C. At the MS1 stage, the mass spectrometer scanned masses in the range of 400–1400 m/z at a resolution of 120 K with an AGC target of 4.0E5 over a 50 ms maximal injection time. At the MS2 stage, ions were fragmented by high-energy collisional dissociation (HCD) with a collision energy of 38% at a detector resolution of 50 K with an AGC target of 1.25E5 (250% relative to default) over a 150 ms maximal injection time, and the Fourier transform first mass mode was fixed at 110 *m/z*.

Proteomics peptide spectrum matching and quantification

Raw MS files were processed by CMSP in Proteome Discoverer v3.0 (Thermo Fisher Scientific, Rockford, IL, USA). Peptide identification was performed by searching HCD MS/MS files against the UniProtKB/Swiss-Prot *mus musculus* database (UP000000589; accessed August 18,

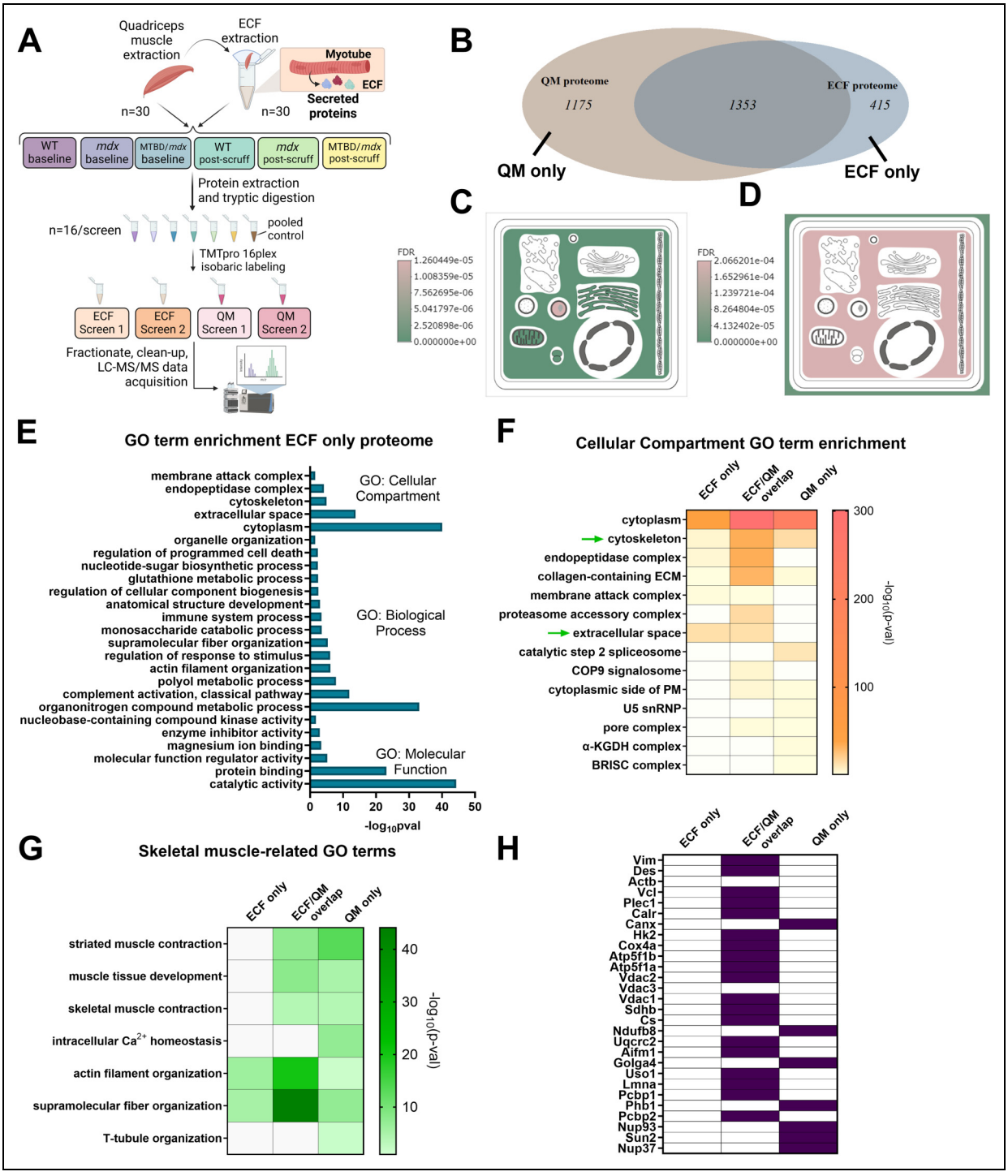

Figure 1. ECF extraction and proteomics analysis revealed enrichment in extracellular and secreted proteins in SkM ECF. (**A**) Schematic representation of experimental design for ECF proteomics analysis, including ECF extraction from quadriceps muscle, sample processing, and data acquisition. (**B**) Venn diagram overlaps reveal proteins identified in the bulk quadriceps muscle (QM) proteome compared to the SkM ECF proteome across all samples. (**C, D**) SubCellularVis[30] schematic representations of cellular compartment enrichment for proteins uniquely identified in the (**C**) QM or (**D**) ECF proteome. (**E**) Bar graph representation of enriched gene ontology (GO) terms associated with proteins identified exclusively in the ECF ("ECF only") proteome. (**F**) Heat map visualization of cellular compartment enrichment in the ECF, QM, and overlapping proteomes. (**G**) Heat map visualization of GO terms related to SkM in the ECF, QM, and overlapping proteomes. (**H**) Visualization of intracellular protein expression from a sample validation list in the ECF, QM, and overlapping proteomes. Illustration in (**A**) made in BioRender.

2023) merged with a common lab contaminant database (https://github.com/HaoGroup-ProtContLib) with the Sequest HT search engine and a 1% false discovery rate (FDR) was set for peptide-to-spectrum matches using the Percolator algorithm in Proteome Discoverer v3.0. The following parameters were used for spectral processing: MS1 tolerance of 20 ppm, MS2 tolerance of 0.08 Da, trypsin (full) digestion with a maximum of two missed cleavage, minimum peptide length of 6 and maximum peptide length of 50, with 10 maximum peptides reported. Cysteine carbamidomethylation was set as a static modification, while TMTpro lysine and N-terminal modifications, asparagine and glutamine deamidation, methionine oxidation, pyroglutamic acid, N-terminal acetylation, methionine-loss, and methionine loss with acetylation were set as dynamic modifications in Sequest. Only protein identifications with high FDR confidence (FDR<1%) and containing 2 or more peptides were accepted. Reporter ion quantification was conducted using the TMTpro 16plex Lot-YD372049 quantification method with a peak integration tolerance of 20 ppm and the most confident centroid method. Unique and razor peptides were used for quantification. All peptides were used for normalization and protein roll-up, and scaling was performed for inter-screen data normalization using a pooled average control sample. Hypothesis testing was performed using ANOVA (individual proteins) for pairwise ratios.

MS bioinformatics analysis

Scaled protein abundances were used to calculate pairwise fold changes based on the geometric means of all biological replicates from each sample group. Fold changes were calculated for pairwise comparisons between the following groups: *mdx* baseline/WT baseline, *mdx* baseline/MTBD-*mdx* baseline, MTBD-*mdx* baseline/WT baseline, *mdx* post-scruff/WT post-scruff, *mdx* post-scruff/MTBD-*mdx* post-scruff, MTBD-*mdx* post-scruff/WT post-scruff, WT post-scruff/WT baseline, *mdx* post-scruff/*mdx* baseline, and MTBD-*mdx* post-scruff/MTBD-*mdx* baseline. A two-way unpaired Student's t-test was used to calculate p-values for pairwise fold changes, and the Benjamini Hochberg method was used to control the false discovery rate (FDR). Corrected p-values were log-transformed and plotted against log-transformed fold change values to obtain volcano plots generated in R using the tidyverse package, and a minimum corrected p-value cutoff of 0.05 and minimum relative fold change cutoff of ± 1 was applied to identify differentially expressed proteins (DEPs) in pairwise comparisons. Comparisons between all experimental groups was performed using two-way ANOVA statistical analysis with Tukey's multiple comparisons correction. Full protein quantification datasets generated in Proteome Discoverer and lists of DEPs were imported to R for data filtering and visualization using the gplots, VennDiagram, and dplyr packages. Venn diagrams were used to obtain lists of overlapping and non-overlapping DEPs between distinct two-group comparisons. DEPs with missing values for two or more biological replicates in an experimental group were excluded from further analysis.

Due to differences in ECF and QM biological matrix effects that impact chromatographic behavior, peptide ionization efficiency, and overall analytical sensitivity during LC-MS data acquisition,[26] we did not design our experiments to quantitatively compare the ECF and QM proteomes. Instead, we qualitatively sorted the ECF and QM proteome datasets to subset ECF-specific and QM-specific proteomes and identify secreted protein candidates that are uniquely present in the SkM ECF.

Functional enrichment analysis was performed using GOrilla,[27] g:Profiler,[28] NaviGO,[29] and SubcellulaRVis for visualization of Gene Ontology Cellular Compartment enrichment.[30] For DEP gene ontology analysis, the target set included the DEP list and the background set included all quantified proteins in the fraction-specific (ECF or QM) proteomics screen. For gene ontology analysis of proteins uniquely represented in ECF or QM proteomes, the compartment-specific dataset was used as the target set, and the Swiss-Prot/UniprotKB[31] Mus musculus reference proteome (dataset downloaded January 15, 2024) was used as the background set. Protein-protein interaction network functional enrichment was performed using STRING (version 12.0). The Swiss-Prot/UniprotKB Mus musculus proteome was filtered for proteins annotated as "secreted" (dataset downloaded December 29, 2024) and was cross-referenced against our proteomics datasets to obtain a subset of candidate secreted proteins. PCA plots were generated in R using the ggfortify package. Pairwise student's t-tests, two-way ANOVA statistical analysis, GO enrichment visualizations, and heat maps for DEPs of interest were performed in GraphPad Prism, version 10.2.

Results

Quadriceps ECF proteome is enriched in extracellular and secreted proteins distinct from bulk quadriceps muscle tissue

To identify novel secreted proteins originating from dystrophin-deficient SkM that may contribute to stress pathology in the *mdx* mouse model of DMD, we employed an ECF isolation technique recently reported by Mittenbuhler et al.[17] Quadriceps SkM was harvested from WT, *mdx*, and MTBD/*mdx* mice expressing transgenic dystrophin in SkM at baseline or 30 min following a 30-s scruff exposure. Quadriceps ECF and ECF-depleted QM from the six experimental groups were subjected to TMTpro 16plex proteomic analysis (Figure 1A).

1768 proteins were quantified in the ECF proteomics screen and 2528 proteins quantified in the QM proteomics screen (Supplemental Data 1 and 2), with 1353 overlapping proteins between the ECF and QM compartments (Figure 1B), representing 76.5% of the ECF proteome and 53.5% of the QM proteome. The overlapping protein dataset, along with the remaining 415 (23.5%) proteins in the ECF-only proteome and 1175 (46.5%) QM-only proteins, were analyzed using gene ontology (GO) enrichment tools to validate the successful isolation of an ECF compartment with extracellular protein enrichment. Cellular compartment enrichment analysis and visualization[30] revealed that the QM only proteome was enriched for intracellular compartments, including cytosol, mitochondria, endoplasmic reticulum, ribosome, and peroxisome (Figure 1C and Table 1). A similar intracellular enrichment was observed in the subset of proteins identified in both ECF and QM matrices (Table 1). Conversely, the ECF only proteome was most enriched for extracellular followed by cytosolic proteins (Figure 1D and Table 1), suggesting that we successfully replicated previous efforts to capture a unique ECF proteome that is likely derived from the extracellular space between muscle cells.[17,20] An orthogonal GO enrichment analysis using the g:GOst enrichment tool in g:Profiler[28] revealed a similar pattern of extracellular protein enrichment in the ECF only proteome (Figure 1E). GO enrichment comparison between compartments demonstrated enrichment of proteins associated with the extracellular space (GO:0005615) exclusively in the ECF only and overlapping proteome subsets and greater enrichment of cytoskeletal proteins (GO:0005856) in the overlapping and QM only proteomes than in the ECF only proteome (Figure 1F). Moreover, biological process GO terms associated with skeletal muscle were significantly overrepresented in the QM only and overlapping proteome subsets but not in the ECF only proteome (Figure 1G). We provided further confirmation of successful ECF compartment isolation by cross-comparing our compartment-specific and overlapping protein datasets with the same test set of common intracellular markers proteins used previously to validate ECF proteomics result.[17] None of the 28 intracellular proteins were found in the ECF-only proteome, while 19/28 intracellular proteins were detected in the overlapping ECF/QM proteome and 7/28 were found in the QM-only proteome (Figure 1H). Our results indicate that exclusion of proteins that overlap between the ECF and QM proteomes is effective in eliminating intracellular proteins and enriching the ECF-only dataset for extracellular and SkM-secreted proteins.

Table 1. Subcellular compartment enrichment in ECF and QM proteomic screens from SubcellulaRVis.

Subcellular Compartment	ECF only proteome (sig $p < 0.05$)	ECF/QM overlapping proteome (sig $p < 0.05$)	QM only proteome (sig $p < 0.05$)
Extracellular region	**0.00**	0.07	1.00
Cytoplasm	**0.00**	**0.00**	**0.00**
Nucleus	1.00	**0.00**	1.00
Golgi apparatus	1.00	1.00	1.00
Vacuole	1.00	0.69	0.96
Cytoskeleton	1.00	**0.00**	0.96
Mitochondrion	1.00	**0.00**	**0.00**
Endoplasmic reticulum	1.00	**0.05**	**0.00**
Endosome	1.00	**0.03**	1.00
Intracellular vesicle	1.00	0.25	1.00
Plasma membrane	1.00	1.00	1.00
Ribosome	1.00	**0.00**	**0.00**
Lysosome	1.00	0.69	0.96
Peroxisome	1.00	**0.00**	**0.00**

Cellular compartment enrichment gene ontology analysis was performed using SubcellulaRVis[30] for proteins in the ECF and QM proteomic screens. A standard enrichment test was performed using the hypergeometric probability function, and p-values were adjusted using the false discovery rate correction.[30] P-values < 0.05 are bolded and represent significantly enriched pathways in the compartment corresponding only to the ECF fraction (ECF only proteome), only to the quadriceps tissue compartment (QM only proteome), or the overlapping ECF and QM compartment (ECF/QM overlapping proteome).

*Dystrophin-deficient bulk SkM and ECF display many upregulated proteins and few downregulated proteins compared to wt or MTBD/*mdx *mice*

Next, we compared protein expression differences between the three genotypes (WT, *mdx*, and MTBD/*mdx*) at baseline to examine dystrophin-dependent proteomic alterations in the quadriceps ECF and QM compartments. Volcano plots were generated to visualize differentially expressed proteins (DEPs) within two-group comparisons (Figure S1 and Figure 2). Compared to the WT ECF proteome at baseline, *mdx* ECF displayed 230 significantly upregulated proteins and 37 downregulated proteins (Figure S1A). In the QM compartment, there were 293 significantly upregulated proteins and 14 significantly downregulated proteins in *mdx* compared to WT quadriceps muscle (Figure S1B). Venn diagrams demonstrate similar basal proteomic alterations in *mdx* skeletal muscle compared with WT or MTBD/*mdx*, regardless of biological compartment (Figure S1C, D). Volcano plot comparisons between *mdx* and MTBD/*mdx* demonstrate 341 upregulated/23 downregulated *mdx* ECF proteins and 329 upregulated/12 downregulated *mdx* QM proteins (Figure S1E, F). One significantly upregulated protein and eight significantly downregulated proteins were observed between MTBD/*mdx* and WT ECF basal proteomes, and no significant differences between MTBD/*mdx* and WT were observed in the QM compartment

(Figure S1G, H), indicating that transgenic expression of the full-length dystrophin/utrophin chimera in skeletal muscle efficiently restores a WT pattern of SkM protein expression and secretion.

Notably, cross-validation of our QM proteomics results against a published *mdx* global proteomics study with similar methodology[32] showed corresponding patterns of differential protein expression between WT and *mdx* skeletal muscle (Table 2 and Supplemental Data 3). Thus, the *mdx* QM proteome in our study exhibits a DMD proteomic signature that is consistent with previous studies,[32,33] but is distinct from the ECF proteome, which yields its own unique pattern of *mdx* proteomic alterations compared with dystrophin-replete controls that may be used to identify novel DMD biomarkers.

Our proteomics analysis also included WT, *mdx*, and MTBD/*mdx* ECF and QM samples collected 30 min after a 30 s exposure to scruff stress (Figure 1A; S2A) to identify myokines that may function as mediators of *mdx* scruff-induced phenotypes. Similar to the *mdx* proteomic landscape at baseline, an abundance of significantly upregulated proteins and relatively fewer downregulated proteins were observed between *mdx* and WT (213 upregulated/66 downregulated) or *mdx* and MTBD/*mdx* (194 upregulated/62 downregulated) after scruff exposure in the ECF compartment (Figure 2A, C). Principal component analysis (PCA) supports these findings and shows that 41.5% of variability (PC1) in the ECF proteomics dataset is attributable to the altered *mdx* proteome, while an additional 12.7% of variability (PC2) may be attributed to differences between the baseline and post-scruff *mdx* proteome (Figure S3A).

Corresponding patterns were observed in post-scruff QM pairwise comparisons, with 139 upregulated/12 downregulated proteins in *mdx* compared to WT quadriceps muscle (Figure 2B) and 142 upregulated/7 downregulated proteins in *mdx* compared to MTBD/*mdx* quadriceps muscle (Figure 2D). In contrast, the WT and MTBD/*mdx* proteomes closely resembled one another (Figure 2E, F). Meanwhile, there were no significant proteomic alterations between the baseline and post-scruff conditions in any genotype (Figure 2G, H; Figure S2B-E). The QM PCA plot demonstrates a subtle effect of scruff stress on the *mdx* QM proteome (Figure S3B), despite the failure of any protein to reach a significant fold-change value (adjusted FDR<0.05) between the *mdx* baseline and post-scruff proteomes (Figure 2H). While proteomic alterations between healthy and dystrophin-deficient SkM and ECF are similar under basal and post-scruff conditions, key differences were highlighted by PCA analysis that suggests the regulation of specific SkM proteins by stress exposure. These alterations are explored throughout the remainder of the manuscript.

*Compensatory changes in the MTBD/*mdx *qm proteome underscore high similarity with wt proteomic status and suggest altered regulation of mRNA processing*

The transgenic MTBD/*mdx* mouse model expresses a full-length dystrophin/utrophin chimera with human skeletal actin (HSA) promoter-driven expression in SkM and dystrophin spectrin-like repeats (SLR) 20–24 in the microtubule (MT) binding domain replaced by utrophin SLR 18–22.[10] Despite this discrepancy between the WT and MTBD/*mdx* dystrophin sequences, only three DEPs were identified between the post-scruff WT and MTBD/*mdx* QM proteomes: peroxiredoxin-2 (PrxII), dipeptidyl peptidase 3, and utrophin (Figure S4A-C). PrxII expression was found to be significantly reduced in *mdx* QM compared to WT in accordance with previous data,[34] but was not restored in MTBD/*mdx* QM (Figure S4A). Dystrophin expression in MTBD/*mdx* QM was fully rescued compared to *mdx* QM and exhibited a non-significant elevated trend compared to WT QM (Figure S4D). Our group previously reported elevated dystrophin expression and unchanged utrophin expression compared to WT, as determined by western blot (WB).[10] Based on this discrepancy between our proteomic and previous WB data, we examined the peptide spectrum matches (PSMs) used for dystrophin and utrophin quantification in our proteomics analysis. We identified 14 PSMs within utrophin SLR 18–22, all of which displayed elevated abundance in MTBD/*mdx* QM compared to WT or *mdx*. Conversely, PSMs identified outside of the SLR 18–22 region in utrophin demonstrated similar or reduced abundance in MTBD/*mdx* compared to WT and *mdx*. Meanwhile, dystrophin PSM inspection revealed a depletion in MTBD/*mdx* PSM abundance (eight PSMs) within the dystrophin SLR 20–24 region, confirming that MTBD/*mdx* SkM expresses a transgenic dystrophin/utrophin chimera and that apparent elevated dystrophin and utrophin levels in MTBD/*mdx* QM are an artefact of omitting the MTBD/*mdx* transgene from the search database during initial data processing.

To confirm the restoration of near-WT protein expression levels in MTBD/*mdx* bulk muscle tissue, we used two-group comparison Venn diagram overlaps to identify baseline QM *mdx* DEPs with altered expression between *mdx* and WT but not between *mdx* and MTBD/*mdx* (intermediate MTBD/*mdx* restoration) and DEPs with altered expression between *mdx* and MTBD/*mdx* but not between *mdx* and WT (compensatory MTBD/*mdx* expression) (Figure S5). See Table 3 for a summary of inter-group DEP comparison terminology. Proteins with intermediate MTBD/*mdx* restoration are those whose levels are altered in *mdx* muscle and incompletely restored in MTBD/*mdx* muscle despite transgenic dystrophin expression. These intermediate DEPs are thus unlikely to be mediators of protection against *mdx* stress susceptibility in MTBD/*mdx* mice. DEP lists were filtered before heatmap

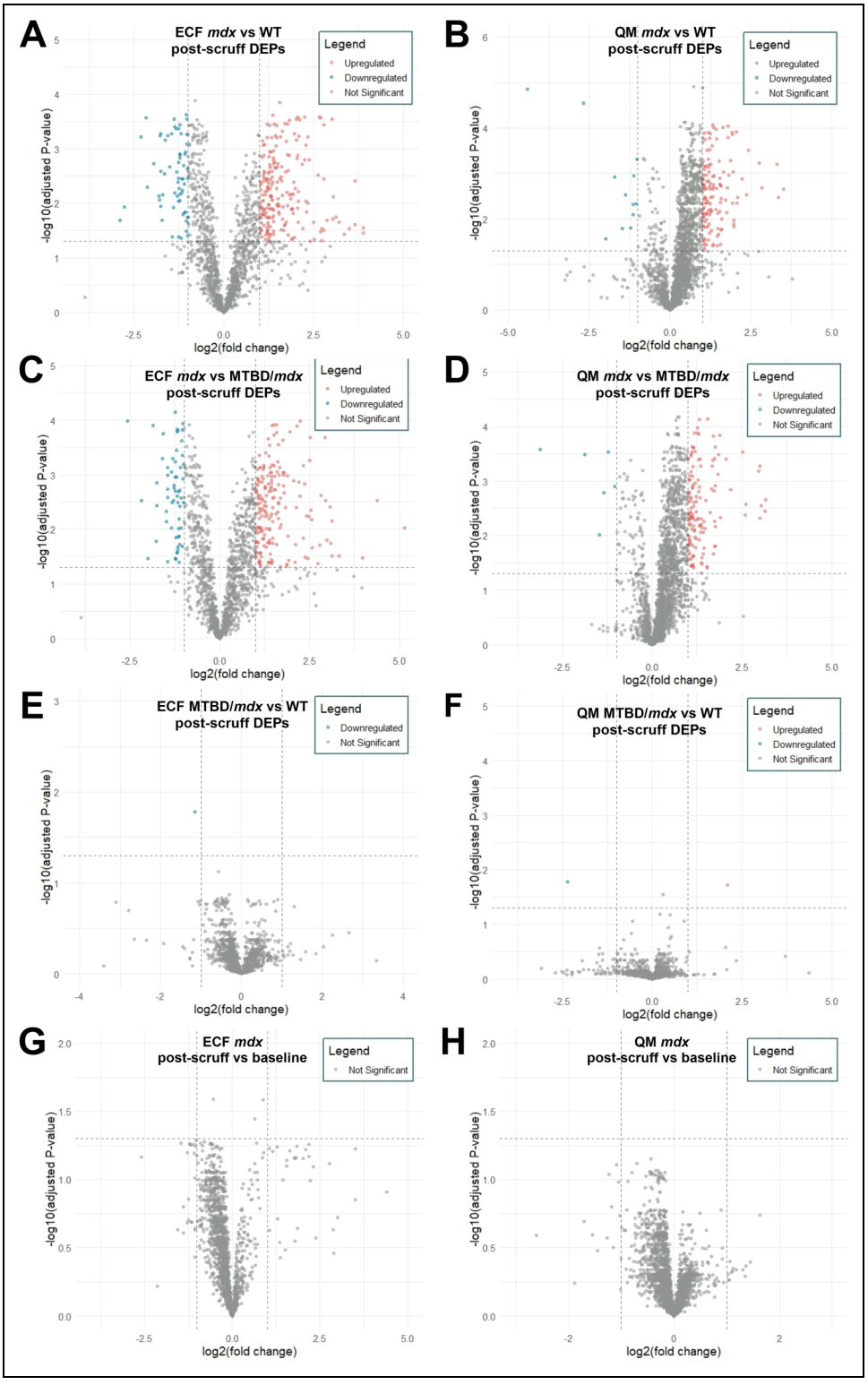

Figure 2. Volcano plots demonstrate stress- and dystrophinopathy-dependent proteomic alterations in qm and ECF compartments. (**A, B**) Volcano plots depict post-scruff *mdx* vs WT comparisons for (**A**) ECF or (**B**) QM proteomes. (**C, D**) Volcano plots depict baseline *mdx* vs MTBD/*mdx* comparisons for (**C**) ECF or (**D**) QM proteomes. (**E, F**) Volcano plots depict baseline MTBD/*mdx* vs WT comparisons for (**E**) ECF or (**F**) QM proteomes. (**G, H**) Volcano plots depict post-scruff vs baseline *mdx* comparisons for (**G**) ECF or (**H**) QM proteomes. Adjusted p-values were determined by Benjamini-Hochberg multiple comparisons hypothesis testing and volcano plots were plot as $\log_2$(fold-change) vs -$\log_{10}$(adjusted p-value).

Table 2. Top *mdx* vs WT differentially expressed proteins (DEPs) in two independent studies.

DEPs *mdx* vs WT (Johnson et al.)	DEPs *mdx* vs MTBD/*mdx* (Johnson et al.)	Common DEPs *mdx* vs WT and *mdx* vs MTBD/*mdx* (Johnson et al.)	DEPs *mdx* vs WT (Day et al.)
↓*Dmd*	**↓*Sspn***	**↓*Dmd***	**↓*Bdh1***
↓*Vps33b*	↓*Pcp4l1*	↓*Vps33b*	↓*Plin5*
↓*Sspn*	**↓*Ces1d***	**↓*Sspn***	↓*Mb*
↓*Dag1*	↓*Amd1*	**↓*Ces1d***	**↓*Dmd***
↓*Sgcg*	↓*H1-0*	**↓*Sgcb***	**↓*Ces1d***
↓*Ces1d*	↓*Vps33b*	↓*H1-0*	↓*Fabp3*
↓*Sgcb*	**↓*Sgcb***	↓*Amd1*	**↓*Sspn***
↓*H1-0*	**↓*Padi2***	**↓*Padi2***	↓*Col2a1*
↓*Amd1*	**↓*Dmd***	↓*Pcp4l1*	**↓*Suclg2***
↓*Cars2*	↓*Utrn*	**↑*Ppia***	↓*Sgcd*
↓*Padi2*	**↓*Bdh1***	**↑*S100a13***	↓*Snta1*
↓*Suclg2*	**↑*Pdia3***	**↑*Lcp1***	↓*Mgst1*
↓*Prdx2*	**↑*Actr3***	**↑*Cstb***	↓*Sod2*
↓*Pcp4l1*	**↑*Hsp90b1***	↑*Pgd*	↓*Ca3*
↑*Ppia*	**↑*S100a13***	**↑*Actr3***	↓*Nos1*
↑*S100a13*	**↑*Cstb***	↑*Clta*	↑*Serpinb1c*
↑*Lcp1*	**↑*Ppia***	**↑*Hsp90b1***	**↑*Lgals3***
↑*Igkc*	**↑*Lcp1***	↑*Add1*	↑*Serpinb1b*
↑*Cstb*	**↑*Vim***	**↑*Serpinb1a***	**↑*Myl6b***
↑*Pgd*	↑*Cap1*	↑*Cap1*	**↑*Lcp1***
↑*Actr3*	↑*Nono*	**↑*Asah1***	↑*Pkhd1l1*
↑*Clta*	**↑*Canx***	↑*Vat1*	↑*S100a4*
↑*Hsp90b1*	**↑*Tmem43***	**↑*Pdia3***	↑*Serpina3g*
↑*Add1*	↑*Arpc2*	**↑*Ppib***	**↑*Ambp***
↑*Serpinb1a*	↑*Clta*	**↑*Vim***	↑*Pls1*
↑*Cap1*	**↑*Cdc42***	**↑*S100a6***	↑*Dock2*
↑*Asah1*	↑*Pgd*	↑*Ahnak*	↑*Mndal*
↑*Vat1*	↑*Ddx39b*	**↑*Eef1a1***	**↑*Lyz2***
↑*Pdia3*	**↑*Basp1***	**↑*Anxa4***	↑*Fcer1g*
↑*Ppib*	↑*Sec11a*	**↑*Pfn1***	**↑*Mustn1***
↑*Vim*	**↑*Lmna***	**↑*Khdrbs1***	**↑*Igkc***
↑*S100a6*	**↑*Esyt1***	**↑*Tmem43***	↑*Tnnc1*
↑*Ahnak*	**↑*Arcn1***	**↑*Esyt1***	**↑*Coro1a***
↑*Eef1a1*	↑*Tkt*	↑*Snx5*	**↑*Hpx***
↑*Anxa4*	**↑*Khdrbs1***	**↑*Coro1b***	**↑*Serpinb1a***

Gene names of top basal differentially expressed proteins (DEPs) between *mdx*, WT, and MTBD/*mdx* SkM in the current study (Johnson et al.) compared with published proteomics data from Day et al. (Supplemental Data 1 in Day et al., 2022).[32] Gene names for downregulated proteins are indicated with a downward-facing arrow (↓), while gene names for upregulated proteins are indicated with an upward-facing arrow (↑). Bolded gene names represent proteins that are altered in common between studies. DEPs across both studies were found to be statistically significant with an adjusted p-value <0.05.

analysis to exclude proteins that were not identified among all replicates within each sample group. Subtle differences were observed between WT and MTBD/*mdx* groups; however, most proteins altered in *mdx* QM were restored by dystrophin expression in MTBD/*mdx* muscle (Figure S5B, S5C). Proteins with altered MTBD/*mdx* expression compared to WT or *mdx* muscle (compensatory proteins) are associated with cellular processes including mRNA processing and striated muscle development (Figure S5D). Interestingly, a small subset of five proteins (bolded gene names) demonstrated similar abundances between WT and *mdx* baseline groups and reduced expression in the baseline MTBD/*mdx* QM compartment, including heat shock protein beta-1 (*Hspb1*; Figure S5E). Thus, our data confirm the near-complete rescue of the MTBD/*mdx* proteome to WT and highlight a handful of intriguing proteomic alterations between WT and MTBD/*mdx* that may regulate mRNA processing, MT network structure, and muscle cell integrity.

Post-scruff ECF mdx *DEPs reveal stress-dependent secreted protein alterations and suggest compensatory redox protein expression in MTBD/*mdx *SkM*

A similar analysis was conducted to analyze pools of intermediate and compensatory expression changes in the MTBD/*mdx* ECF proteome compared to WT and *mdx*

Table 3. Inter-group DEP comparison terminology.

Terminology for Inter-Group DEP Comparisons		
Term	Inter-group relative expression levels	Description
Intermediate MTBD/*mdx* restoration	MTBD/*mdx* = *mdx* < or > WT	Protein levels altered in *mdx* muscle and incompletely restored in MTBD/*mdx* muscle
Rescued MTBD/*mdx* expression	MTBD/*mdx* = WT < or > *mdx*	Protein levels altered in *mdx* muscle and restored in MTBD/*mdx* muscle
Compensatory MTBD/*mdx* expression	MTBD/*mdx* < or > *mdx* = WT	Protein levels altered in MTBD/*mdx* muscle compared to *mdx* and WT muscle

Summary table for relative expression levels of intermediate, rescued, and compensatory protein expression levels in MTBD/*mdx* extracellular fluid or quadriceps muscle.

ECF following scruff exposure (Figure 3A). This analysis did not reveal major differences between the WT and MTBD/*mdx* post-scruff ECF proteomes (Figure 3B, C), but did draw out secreted protein candidates (bolded gene names in Figure 3B, C) that were reduced in *mdx* post-scruff ECF and may be related to *mdx* scruff pathology, including adiponectin (*Adipoq*; Figure 3D, E), calreticulin (*Calr*), and myeloid-derived growth factor (*Mydgf*). Additionally, comparison of *mdx* and healthy SkM ECF revealed diminished levels of antioxidant defense enzymes including glutathione S-transferase 1 (*Gstm1*), glutathione S-transferase 2 (*Gstm2*), and glutaredoxin (*Glrx*) in *mdx* ECF that were rescued back to WT levels in MTBD/*mdx* ECF (Figure 3C, F). Notably, glutathione S-transferase 1 (Figure 3G) abundance in the QM compartment was significantly elevated in MTBD/*mdx* SkM above WT and *mdx* levels, perhaps as an aspect of improved antioxidant function with restored SkM dystrophin expression.[32,34] Altogether, these data do not suggest substantial differences between the WT and MTBD/*mdx* ECF proteome, but do reveal secreted and redox-regulatory protein factors that should be further investigated as contributors to *mdx* stress pathology and physiological stress susceptibility.

Compartment-specific proteomic enrichment analysis reveals stress-dependent myokine candidates in mdx *SkM ECF*

We previously showed that MTBD/*mdx* mice exhibit WT-level protection against scruff-induced hypotension and inactivity.[8,9] Therefore, secreted myokine candidates that modulate scruff susceptibility in *mdx* mice are expected to be restored to WT-level expression in MTBD/*mdx* mice. Our experimental design allowed us to isolate the ECF fraction with greater enrichment in secreted proteins than intact muscle tissue. To identify secreted protein candidates with differential expression between WT, *mdx*, and MTBD/*mdx*, we filtered lists of DEPs by biological compartment: *mdx* DEPs in the ECF proteomics dataset also found in the QM dataset were excluded to obtain an ECF only dataset, and vice versa to obtain a QM only dataset. This filtering step produced an enrichment in extracellular and secreted proteins among *mdx* DEPs in the ECF compartment at baseline (Figure 4A) and after scruff exposure (Figure 4B). Filtering by the QM only proteome resulted in no significant enrichment of any compartment among *mdx* QM DEPs. Venn diagrams in Figure 5A and 5C were used to identify *mdx* baseline and post-scruff DEPs. We further filtered our DEP lists to exclude proteins that were not identified among all replicates within each sample group to obtain a robust set of secreted protein candidates relevant to *mdx* scruff pathology. After filtering, there were 12 significantly altered proteins in *mdx* ECF compared with WT or MTBD/*mdx* at baseline, while scruff exposure altered expression of five additional proteins in *mdx* ECF (Figure 5B). In the QM compartment, 25 DEPs were identified in *mdx* SkM compared to WT or MTBD/*mdx* at baseline, and one DEP was identified in *mdx* SkM compared to WT or MTBD/*mdx* after scruff stress (Figure 5D).

We overlaid our DEP datasets with the reviewed Swiss-Prot dataset containing secreted protein annotations (UniProtKB search term: cc_scl_term:SL-0243; downloaded January 2024) to identify secreted SkM DEP candidates, which are represented by the bolded terms in the ECF and QM DEP heatmaps (Figure 5B, D) and listed in Table 4. Three secreted proteins were identified among the DEPs in *mdx* QM at baseline (Figure 6A), while there were no DEPs annotated as secreted in the post-scruff *mdx* QM compartment. Eight secreted proteins were identified among the DEPs in *mdx* ECF at baseline (Figure 6B), a subset of which were also elevated in *mdx* post-scruff ECF to varying extents. A singular protein, follistatin-like 1 protein (*Fstl1*; FSTL1) was returned as a secreted protein that was detected solely in the ECF proteome with significant differential expression in *mdx* ECF after scruff exposure in two-group comparisons against WT or MTBD/*mdx* ECF (Figure 6C; Table 4). Two-way ANOVA statistical comparison of all six experimental groups indicated significantly elevated FSTL1 protein abundance in *mdx* ECF at baseline and post-scruff, with a non-significant trend (interaction term p-value = 0.06) toward further elevation in *mdx* post-scruff ECF (Figure 6C). Predictive linear regression analysis revealed a significant negative correlation between post-scruff activity levels and FSTL1 abundance in ECF (Figure 6D; $R = -0.746$; $R^2 = 0.558$; $p = 0.0014$), suggesting

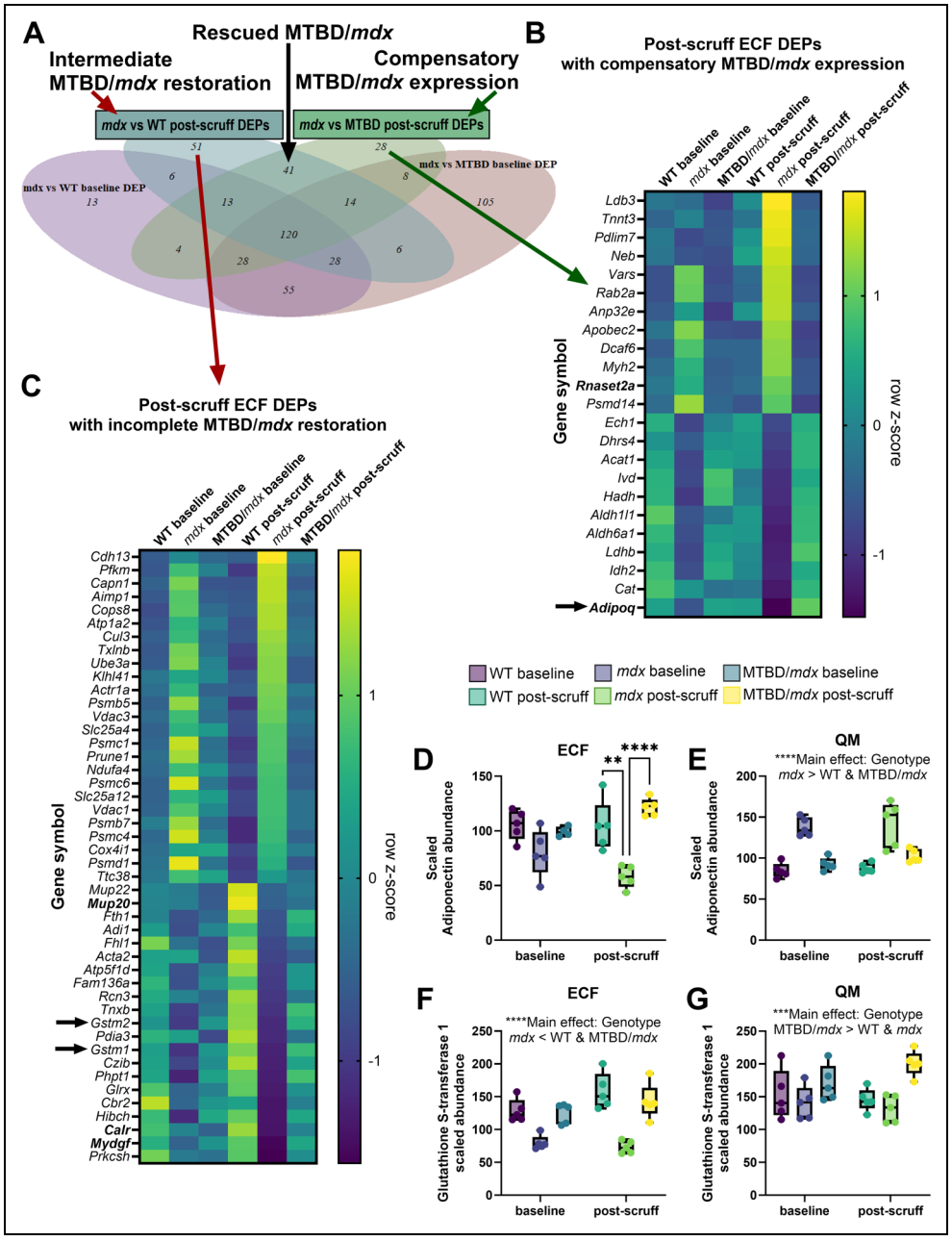

Figure 3. Compensatory and unaltered post-scruff proteomic alterations in MTBD/*mdx* compared to *mdx* ECF. (**A**) Venn diagram displays overlapping DEPs between two-group comparisons of *mdx* vs WT and *mdx* vs MTBD/*mdx* in ECF compartment at baseline and following scruff exposure. Compensatory proteins are identified as *mdx* vs MTBD/*mdx* DEPs that are not differentially expressed between *mdx* and WT. Proteins that exhibit intermediate MTBD/*mdx* restoration are considered as *mdx* vs WT DEPs that are also differentially expressed between MTBD/*mdx* and WT. (**B**) Heat map visualization of post-scruff ECF proteins that display compensatory expression in MTBD/*mdx* ECF compared to *mdx* and WT groups (*mdx* vs MTBD/*mdx* post-scruff DEPs that do not overlap with *mdx* vs WT baseline or post-scruff DEPs or *mdx* vs MTBD/*mdx* baseline DEPs). Bolded proteins are annotated as secreted in the Uniprot database. (**C**) Heat map visualization of post-scruff ECF proteins that are not rescued or demonstrate intermediate expression in MTBD/*mdx* ECF compared to *mdx* and WT ECF (*mdx* vs WT post-scruff DEPs that do not overlap with *mdx* vs WT baseline or *mdx* vs MTBD/*mdx* baseline or post-scruff DEPs). Bolded proteins are annotated as secreted in the Uniprot database. (**D**, **E**) Adiponectin (*Adipoq*) abundance in WT, *mdx*, and MTBD/*mdx* baseline and post-scruff (**D**) ECF and (**E**) QM samples. (**F**, **G**) Glutathione S-transferase 1 (*Gstm1*; GSTM1) abundance in WT, *mdx*, and MTBD/*mdx* baseline and post-scruff (**F**) ECF and (**G**) QM samples. Heat map z-scores were calculated as group z-score averages using the row mean and population standard deviation for each protein. Box plots depict minimum, Q1, median, Q3, and maximum values from n = 5 mice/group. . Comparisons between groups were made using two-way ANOVA with Tukey's multiple comparisons test (*$p < 0.05$; **$p < 0.01$; ***$p < 0.001$; ****$p < 0.0001$).

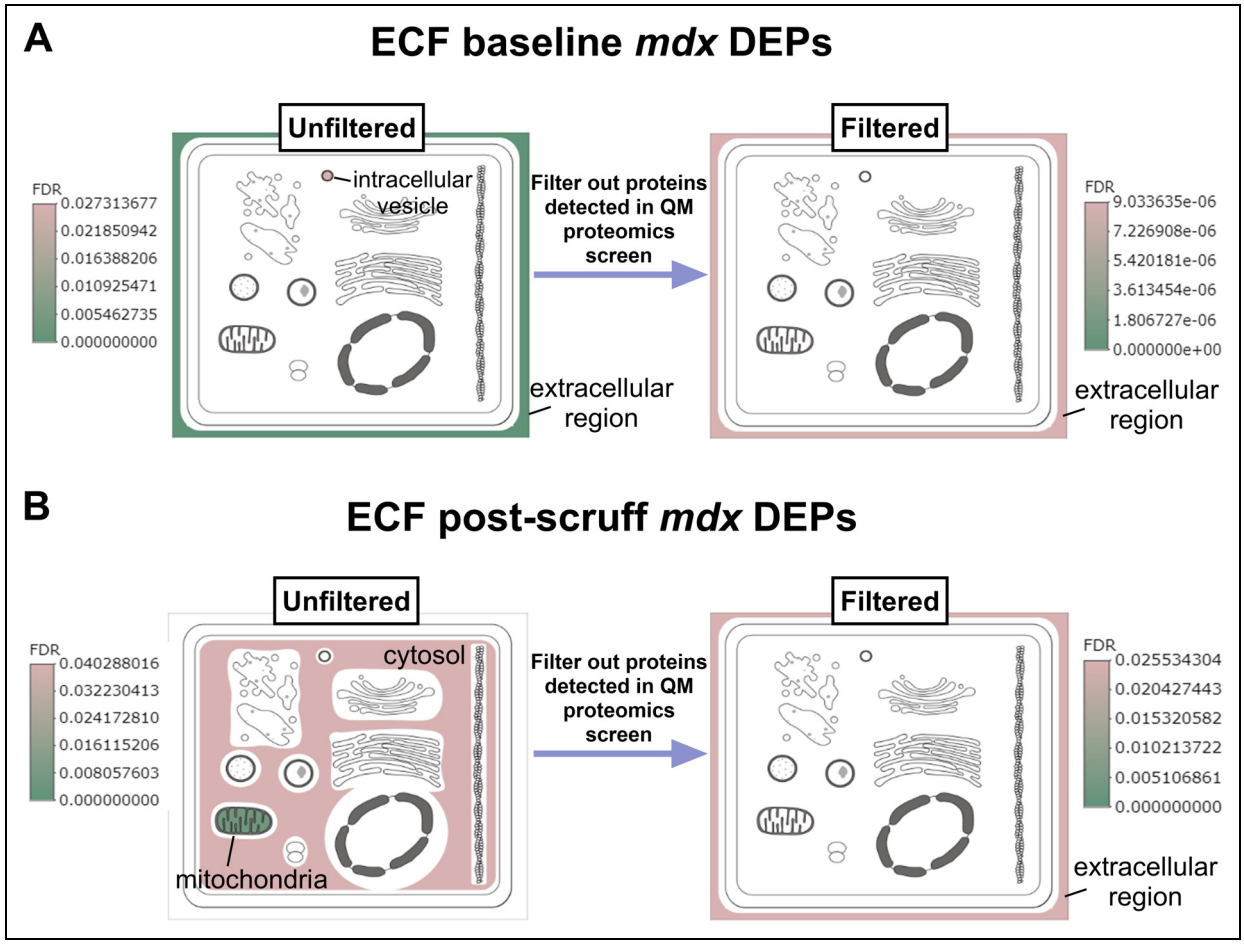

Figure 4. Cellular compartment enrichment analysis demonstrates successful data filtering to enrich ECF secreted protein list. (**A, B**) SubcellularVis[30] compartment enrichment analysis and graphical depictions for (**A**) ECF baseline *mdx* DEP list and (**B**) ECF post-scruff *mdx* DEP list before and after the removal of proteins also identified in the QM proteome.

that elevated FSTL1 may be a compelling predictive biomarker of stress susceptibility in *mdx* mice or that stress exposure leads to elevated FSLT1 secretion in SkM. GO enrichment analysis was performed for the small suite of secreted proteins identified as basally elevated in *mdx* ECF compared to WT or MTBD/*mdx* mice, which revealed significant enrichment in extracellular compartment localization, immune response, complement activation, protein activation cascade, and extracellular structure organization (Figure 6E).

FSTL1 expression is elevated in mdx *circulation and reduced in* mdx *ECF-depleted quadriceps muscle*

Stress-induced alterations in *mdx* FSTL1 expression in quadriceps muscle and plasma were further validated with orthogonal techniques, including real-time quantitative PCR, WB, and enzyme-linked immunosorbent assay (ELISA). We demonstrated that *Fstl1* mRNA levels were not significantly increased in *mdx* quadriceps muscle (Figure 7A; main effect p-value = 0.05), corresponding to similar FSTL1 protein levels between WT, *mdx*, and MTBD/*mdx* quadriceps muscle at baseline and after scruff exposure, as determined by WB (Figure 7B, C). Immunoblotting for FSTL1 protein revealed multiple bands at the expected FSTL1 molecular weight (35 kDa), as well as several bands between 37 and 50 kDa (Figure 7B, C). Three N-glycosylation sites and two O-glycosylation sites have been identified for FSTL1.[22] Published FSTL1 WB data in mouse adipose tissue and cell culture lysates reports a glycosylated FSTL1 band at 55 kDa, non-glycosylated FSTL1 band at 40 kDa, and a hypo-glycosylated FSTL1 band between 40 and 55kDa.[35] Therefore, multiple putative glycosylated FSTL1 bands were detected in our analysis between 37 and 50 kDa and were grouped together for comparison with non-glycosylated FSTL1 at 35 kDa. The FSTL1 glycosylation status was not significantly different between groups at baseline or after scruff exposure (Figure 7B, C).

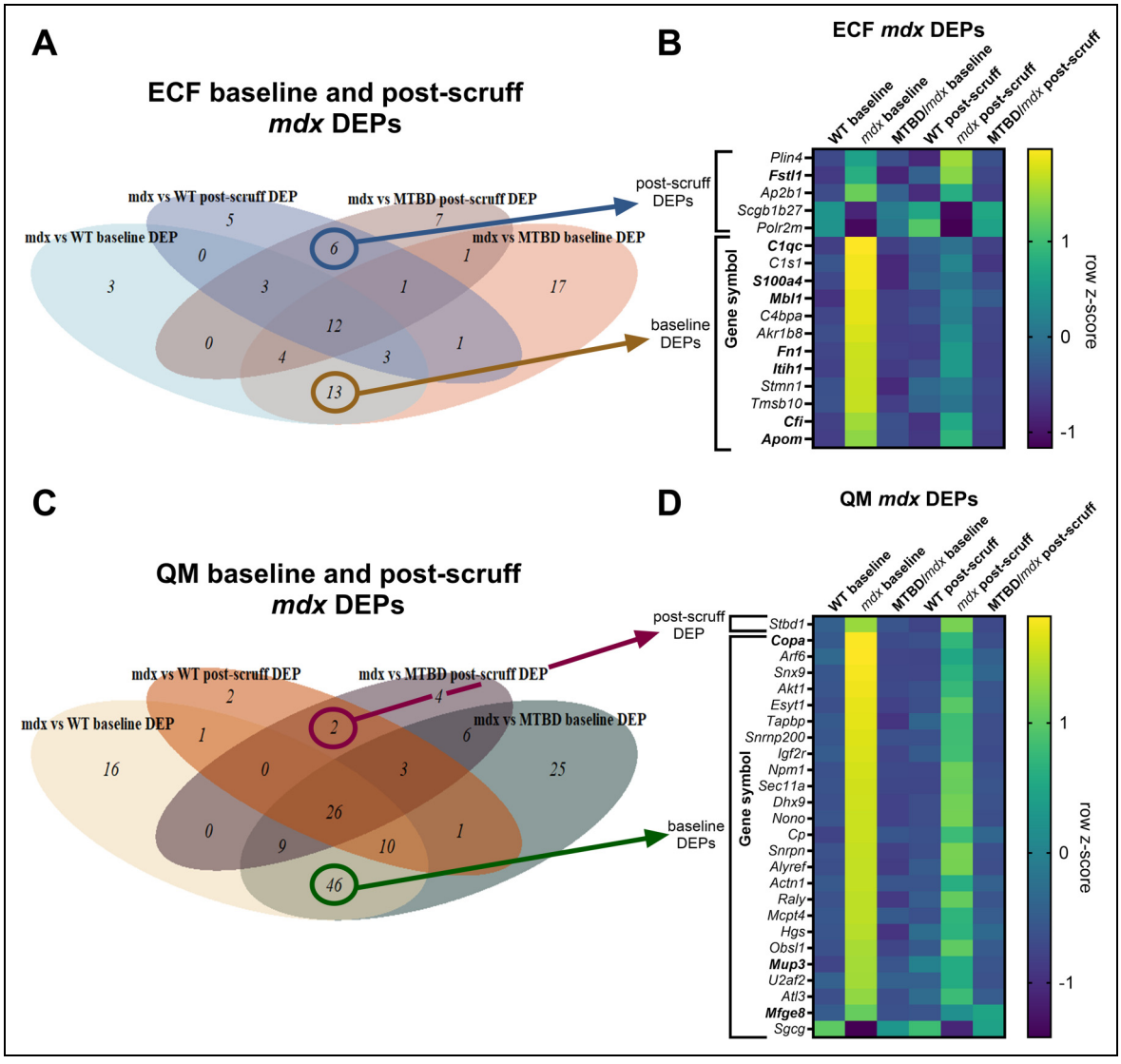

Figure 5. Compartment-specific proteomic enrichment analysis identifies stress-and dystrophinopathy-dependent myokines in *mdx* SkM ECF. (**A**) Venn diagram depicts proteome overlaps between *mdx* DEP two-group comparisons identified exclusively in the ECF compartment. (**B**) Heat map visualization of baseline and post-scruff *mdx* DEPs identified exclusively in the ECF compartment (ECF *mdx* vs MTBD/*mdx* DEPs that overlap with *mdx* vs WT DEPs after excluding proteins also found in the QM proteome), filtered to exclude proteins with missing values across replicates. (**C**) Venn diagram depicts proteome overlaps between *mdx* DEP two-group comparisons identified exclusively in the QM compartment. (**D**) Heat map visualization of baseline and post-scruff *mdx* DEPs identified exclusively in the QM compartment (QM *mdx* vs MTBD/*mdx* DEPs that overlap with *mdx* vs WT DEPs after excluding proteins also found in the ECF proteome), filtered to exclude proteins with missing values across replicates. Heat map z-scores were calculated as group z-score averages using the row mean and population standard deviation for each protein.

In contrast, FSTL1 quantification with a commercial ELISA kit (CusaBio, Wuhan, China) demonstrated reduced FSTL1 levels in *mdx* quadriceps muscle at baseline and after scruff exposure, with a mild post-scruff reduction in SkM FSTL1 levels across groups (Figure 7D). ELISA quantification of FSTL1 in quadriceps-derived ECF samples analyzed in the ECF proteomics screen also demonstrated reduced *mdx* FSTL1 levels at baseline and post-scruff (Figure 7E). Circulating FSTL1 levels in *mdx* plasma were determined to be elevated by ELISA analysis, with a more dramatic elevation at baseline than after scruff exposure (Figure 7F). These immunoassay-based results contrast with one another and with the elevation in *mdx* FSTL1 levels reported by SkM ECF proteomics analysis (Figure 6C). The apparent discrepancy between FSTL1 detection methods may be related to the variable post-translational glycosylation modifications on FSTL1 and a higher avidity for certain glycosylated FSTL1 states over

Table 4. Putative myokines with altered levels in the *mdx* skeletal muscle secretome.

DEP Category	Gene/Protein Name	Uniprot ID	*mdx*/WT fold-change ECF baseline	*mdx*/WT fold-change ECF post-scruff
Secreted ECF Baseline DEPs	*S100a4*/Protein S100-A4	P07091	2.06	1.08
	C1qc/Complement C1q subcomponent subunit C	Q02105	3.36	1.15
	Mbl1/Mannose-binding protein A	P39039	2.22	1.31
	C4bpa/C4b-binding protein	P08607	2.86	1.41
	Itih1/Inter-alpha-trypsin inhibitor heavy chain H1	Q61702	2.30	1.50
	Cfi/Complement factor I	Q61129	4.03	3.55
	Apom/Apolipoprotein M	Q9Z1R3	8.06	5.39
	Fn1/Fibronectin	P11276	3.68	2.47

DEP Category	Gene/Protein Name	Uniprot ID	*mdx*/WT fold-change ECF baseline	*mdx*/WT fold-change ECF post-scruff
Secreted ECF Post-Scruff DEP	*Fstl1*/follistatin-like 1 protein	Q62356	1.85	2.14

DEP Category	Gene/Protein Name	Uniprot ID	*mdx*/WT fold-change QM baseline	*mdx*/WT fold-change QM post-scruff
Secreted QM Baseline DEPs	*Copa*/Coatomer subunit alpha	Q8CIE6	2.03	1.63
	Mfge8/Lactadherin	P21956	2.31	1.87
	Mup3/Major urinary protein 3	P04939	2.99	1.32

Listed proteins have been annotated as secreted in the UniProtKB database and are differentially expressed in *mdx* ECF or QM compartments compared to WT or MTBD/*mdx* at baseline or after scruff stress exposure, suggesting potential altered myokine profiles in the *mdx* SkM secretome.

others. A strength of our discovery proteomics approach is the aversion of bias associated with antibody binding and interference effects, as well as the ability to quantify proteins indiscriminate of glycosylation status or other post-translational modification events.

Overlapping proteome analysis demonstrates secretion of contractile SkM proteins from mdx *quadriceps muscle upon stress exposure*

In addition to secreted proteins found exclusively in the extracellular compartment, our SkM ECF protein list contained a considerable number of proteins that are also found in intracellular compartments.[17] Therefore, we extended our ECF proteomics data analysis to include proteins with overlapping identification in the ECF and QM proteomes (Figures 8, S6). Venn diagram overlaps for two-group comparison DEP lists reveal 42 proteins with differential expression between *mdx* and WT or MTBD/*mdx* SkM ECF at baseline and 35 proteins identified uniquely in a post-scruff condition (Figure 8A). None of the post-scruff ECF DEPs were annotated as secreted in the UniProt database. Subcellular compartment enrichment analysis revealed cytosolic and mitochondrial enrichment in post-scruff ECF DEPs (Figure 8B), while baseline DEPs were enriched for the cytosol, extracellular space, and intracellular vesicles (Figure 8C). Further filtering was performed to retain 25 post-scruff ECF DEPs identified in all samples, whose abundances in the ECF and QM compartments are displayed by heatmap in Figure 8D. Of these, ten proteins were identified with unique elevation in *mdx* ECF after scruff exposure (Figure 8D).

Intriguingly, post-scruff protein expression changes in *mdx* ECF do not appear to be mirrored in *mdx* bulk SkM tissue, as demonstrated by the subtle pattern of expression changes for proteins in the QM compartment that were dramatically elevated or reduced in the ECF compartment after scruff exposure (Figure 8D). In contrast, proteins uniquely altered in *mdx* QM at baseline displayed a similar pattern of elevation after scruff (Figures S6A, B), and proteins with altered basal expression in *mdx* ECF were similarly altered after scruff and in the QM compartment (Figure S6C). These expression patterns suggest a unique subset of proteins with dramatically increased abundance in the *mdx* ECF compartment after scruff stress exposure that may be actively secreted from SkM to regulate the

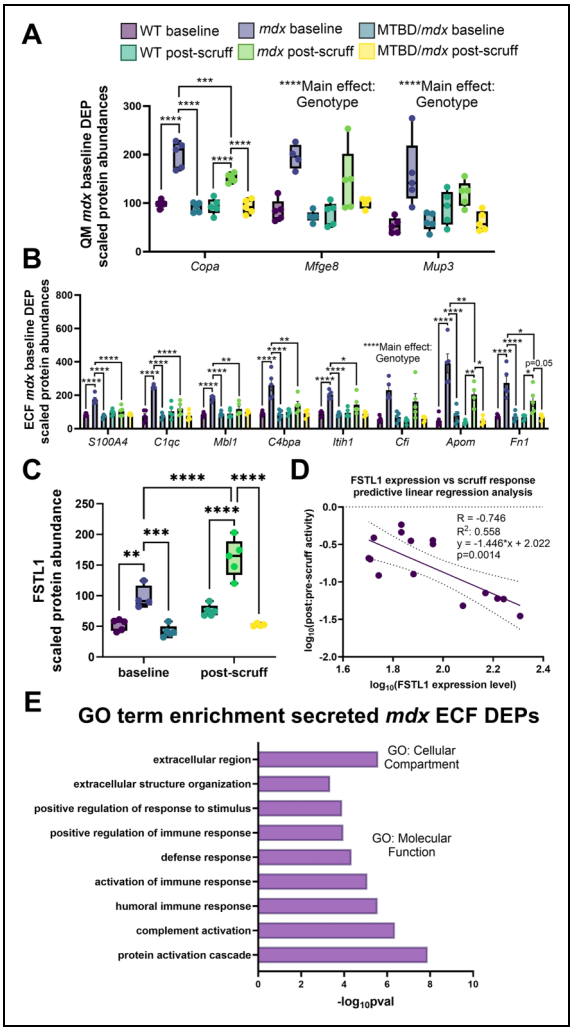

Figure 6. Scruff- and dystrophinopathy-dependent QM and ECF DEP analysis. (**A**) Proteomic quantification of QM baseline *mdx* DEPs includes COPI coat complex subunit alpha (*Copa*), lactadherin (*Mfge8*), and major urinary protein 3 (*Mup3*). (**B**) Proteomic quantification of ECF baseline *mdx* DEPs includes S100 calcium binding protein A4 (*S100A4*), complement C1q C chain (*C1qc*), mannose-binding lectin 1 (*Mbl1*), complement component 4 binding protein alpha (*C4bpa*), inter-alpha-trypsin inhibitor heavy chain 1 (*Itih1*), complement factor I (*Cfi*), apolipoprotein M (*Apom*), and fibronectin (*Fn1*). (**C**) FSTL1 levels are shown for WT, *mdx*, and MTBD/*mdx* baseline and post-scruff SkM ECF. (**D**) Predictive linear regression analysis was performed to quantify the strength of correlation between FSTL1 levels in SkM ECF and magnitude of scruff-induced inactivity in WT, *mdx*, and MTBD/*mdx* mice. A simple linear regression analysis was performed on $\log_{10}$-transformed FSTL1 abundance and post:pre-scruff activity ratios to fit a line with equation ($y = -1.446*x + 2.022$) with $R = -0.746$, $R^2 = 0.558$, and a slope that was statistically significantly non-zero ($p = 0.0014$) by an F-test ($F = 16.39$; $DFn = 1$; $DFd = 13$). (**E**) Bar graph representation of enriched gene ontology (GO) terms associated with secreted ECF DEPs. Box plots depict minimum, Q1, median, Q3, and maximum values from $n = 5$ mice/group. Comparisons between groups were made using two-way ANOVA with Tukey's multiple comparisons test (*$p < 0.05$; **$p < 0.01$; ***$p < 0.001$; ****$p < 0.0001$).

mdx central stress response. DEPs with significantly elevated post-scruff abundance exclusively in *mdx* ECF included myosin-binding protein C, fast-type (*Mybpc2*; fast MyBP-C), junctophilin-1 (*Jph1*; JP-1), junctophilin-2 (*Jph2*; JP-2), myomesin 2 (*Myom2*), and tropomyosin alpha-1 chain (*Tpm1*) (Figure 8D). GO enrichment analysis revealed that these post-scruff ECF DEPs are found in contractile fibers and junctional membrane complexes and serve as structural components of the cytoskeleton (Figure 1E). JP-1 expression in ECF and QM compartments is representative of the trend in elevated post-scruff ECF DEPs, with significantly increased JP-1 abundance in *mdx* post-scruff ECF and no differences in JP-1 abundance between any groups in QM (Figure 9A). Similar to FSTL1, JP-1 abundance in the ECF compartment significantly negatively correlates with post-scruff inactivity (Figure 9B; $R = -0.736$; $R^2 = 0.542$; $p = 0.0018$), indicating that JP-1 may serve as an additional biomarker for *mdx* stress vulnerability. Our data introduce the possibility that contractile proteins are secreted from *mdx* SkM during scruff exposure, a mild form of stress that induces *mdx* hypoactivity.

Discussion

Our ECF proteomics investigation revealed distinct patterns of protein secretion from *mdx* SkM compared to WT and dystrophin-replete MTBD/*mdx* SkM, along with a subset of stress-dependent proteomic alterations that are most prominent in *mdx* SkM ECF. Some of the ECF *mdx* DEPs identified at baseline are associated with inflammation and intracellular calcium regulation, several of which have been previously identified as differentially expressed in *mdx* SkM, including protein S100-A4,[33] fibronectin,[33,36] complement C1q subcomponent C,[37] and C4b-binding protein.[38] Mannose-binding protein A, complement C1q subcomponent subunit C, and complement factor I are all part of the complement system also involved in altered immune responses within dystrophin-deficient muscle.[39] Apolipoprotein M expression has not been reported as altered in DMD. However, fatty acid binding protein 3 levels are reduced in DMD SkM compared to Becker muscular dystrophy or healthy SkM, while apolipoprotein A-I levels are increased,[40] suggesting dysregulated lipid metabolism in *mdx*/DMD SkM and circulation.[41,42] Our finding that fibronectin is over-secreted from *mdx* SkM agrees with an earlier characterization of the SkM secretome in cultured *mdx* myotubes[43] and extends these previous findings to include a novel panel of *mdx* myokines identified *ex vivo* in SkM tissue. FSTL1 was not detected in the quadriceps QM compartment, but was elevated in *mdx* ECF at baseline and after scruff exposure, with a trend toward further elevation in the post-scruff condition, and exhibited restored WT expression in MTBD/*mdx* ECF. Although volcano plot analysis did not highlight a significant

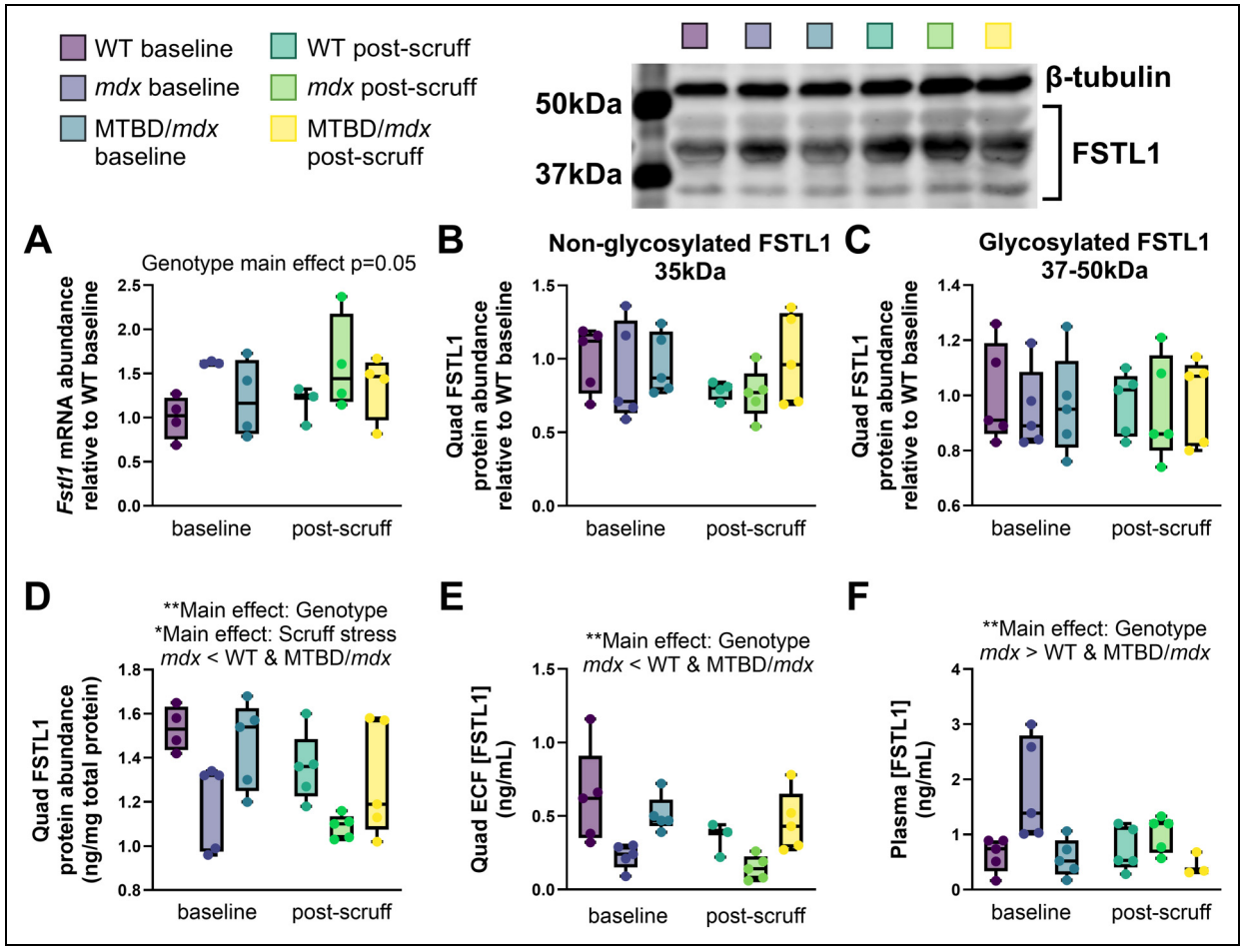

Figure 7. Orthogonal validation of FSTL1 expression in SkM, ECF, and plasma. (**A**) Transcript abundance of *Fstl1* was quantified by qRT-PCR in WT, *mdx*, and MTBD/*mdx* baseline and post-scruff quadriceps muscle. (**B, C**) FSTL1 protein bands corresponding to (**B**) non-glycosylated and (**C**) glycosylated molecular weights were quantified by WB and normalized to β-tubulin content in WT, *mdx*, and MTBD/*mdx* baseline and post-scruff quadriceps muscle. (**D-F**) FSTL1 protein expression was quantified by ELISA in WT, *mdx*, and MTBD/*mdx* baseline and post-scruff (**D**) quadriceps muscle, (**E**) ECF, and (**F**) plasma. Box plots depict minimum, Q1, median, Q3, and maximum values from n = 5 mice/group. Comparisons between groups were made using two-way ANOVA with Tukey's multiple comparisons test (*p < 0.05; **p < 0.01; ***p < 0.001; ****p < 0.0001).

elevation in FSTL1 between *mdx* post-scruff and baseline conditions, the fold-change thresholds and multiple hypothesis testing corrections applied to the dataset may have been too stringent to identify patterns that emerge from more focused investigation of smaller data subsets of high experimental relevance. Interestingly, FSTL1 levels moderately correlated with the magnitude of post-scruff inactivity in WT, *mdx*, and MTBD/*mdx* mice ($R^2 = 0.558$), suggesting that FSTL1 may be a useful stress biomarker and possible signaling factor in the stress response pathway that modulates *mdx* scruff-induced inactivity.

FSTL1 is a glycoprotein in the secreted protein acid and rich in cysteine (SPARC) family and is an established myokine that has been implicated in exercise response,[44–46] endothelial cell proliferation,[47] BMP and TGFβ signaling, cardiovascular disease, and a number of other disease mechanisms.[22,48,49] FSTL1 exhibits proliferative and regenerative capacities, as well as pro-inflammatory and pro-tumorigenic functions depending on disease state, cell type-specific regulation of expression, post-translational glycosylation, and activation of diverse signaling pathways.[21,22] Previously, Zhou et al. observed elevated *Fstl1* mRNA levels in *mdx* mice that were further increased in DKO mice lacking both dystrophin and utrophin.[50] Elevated FSTL1 levels correlate with chronic unpredictable mild stress exposure in mice and genetic *Fstl1* knockdown reversed depression- and anxiety-like behaviors as well as defects in synaptic plasticity in stress-exposed mice through microglial TLR4/MyD88/NF-κB signaling.[23] FSTL1 has also been shown to be upregulated as a pro-inflammatory signaling molecule in chronic immune disease conditions such as arthritis and Kawasaki disease.[22,51] Pro-fibrotic signaling functions for FSTL1[52] may be particularly relevant to the elevated fibrotic SkM

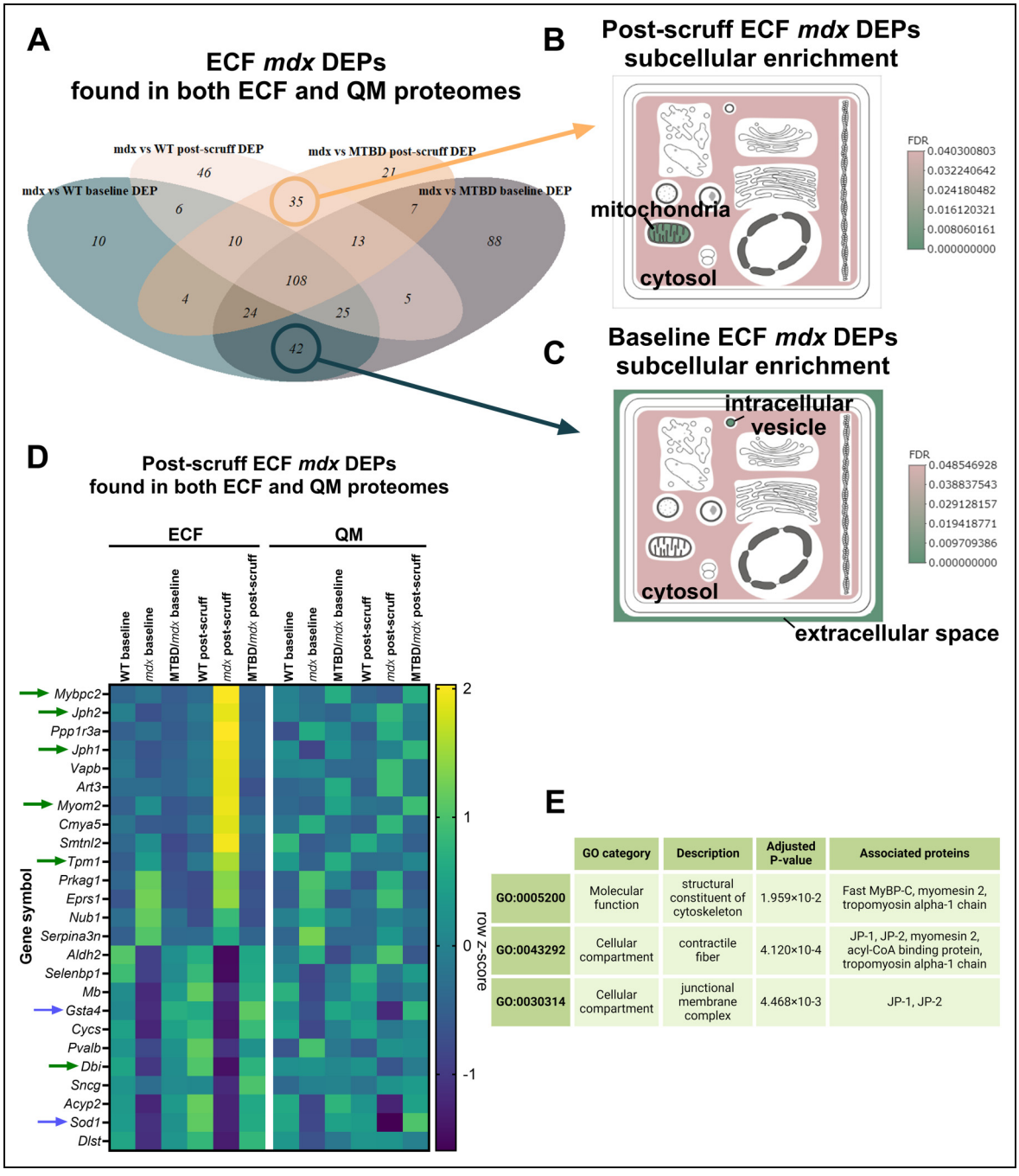

	GO category	Description	Adjusted P-value	Associated proteins
GO:0005200	Molecular function	structural constituent of cytoskeleton	1.959×10-2	Fast MyBP-C, myomesin 2, tropomyosin alpha-1 chain
GO:0043292	Cellular compartment	contractile fiber	4.120×10-4	JP-1, JP-2, myomesin 2, acyl-CoA binding protein, tropomyosin alpha-1 chain
GO:0030314	Cellular compartment	junctional membrane complex	4.468×10-3	JP-1, JP-2

Figure 8. Contractile and cytoskeletal SkM proteins are elevated in *mdx* SkM ECF upon stress exposure. (**A**) Venn diagram analysis demonstrates overlapping *mdx* DEPs between baseline and post-scruff conditions within the ECF proteome that overlap with the QM proteome. (**B, C**) SubcellularVis[30] compartment enrichment analysis and graphical depictions for (**B**) ECF post-scruff *mdx* DEP list (*mdx* vs MTBD/*mdx* post-scruff DEPs that overlap with *mdx* vs WT post-scruff DEPs), and (**C**) ECF baseline *mdx* DEP list (*mdx* vs MTBD/*mdx* baseline DEPs that overlap with *mdx* vs WT baseline DEPs) filtered by protein detection in both ECF and QM proteomic screens. (**D**) Heat map visualization of relative protein abundance in ECF and QM compartments for ECF post-scruff DEP list filtered by protein detection in both ECF and QM proteomic screens. (**E**) Table of enriched GO terms associated with *mdx* post-scruff ECF DEPs. Heat map z-scores were calculated as group z-score averages using the row mean and population standard deviation for each protein.

phenotype of *mdx* mice that are exposed to chronic daily scruff stress.[53] Thus, FSTL1 is actively secreted by skeletal muscle under numerous physiological states, promotes inter-organ crosstalk, particularly within the cardiovascular and central nervous system, and is known to be upregulated in chronic inflammatory conditions

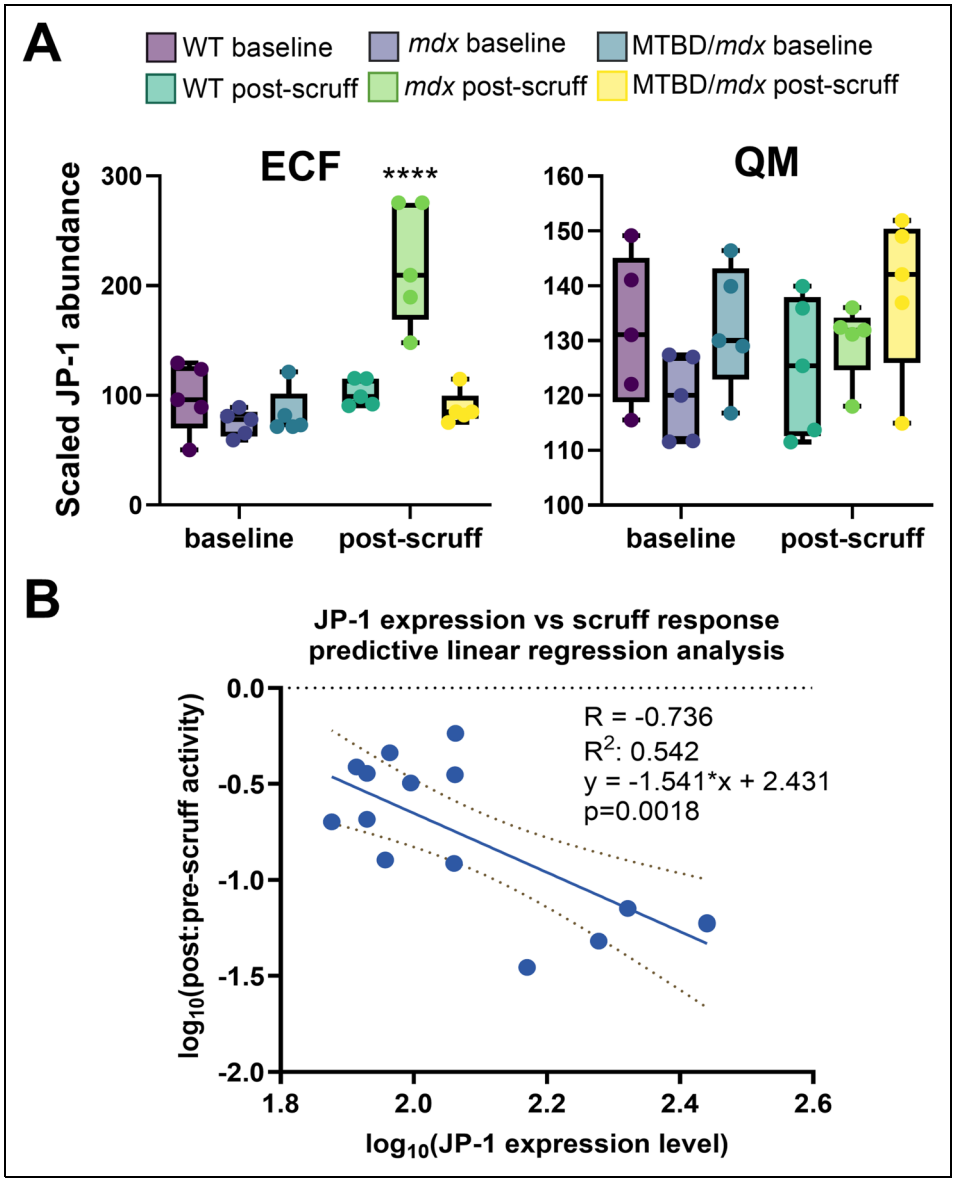

Figure 9. Junctophilin-1 is elevated in *mdx* SkM ECF upon stress exposure. (**A**) Junctophilin-1 (JP-1) protein abundance in WT, *mdx*, and MTBD/*mdx* baseline and post-scruff ECF and QM samples. (**B**) Predictive linear regression analysis was performed to quantify the strength of correlation between JP-1 levels in SkM ECF and magnitude of scruff-induced inactivity in WT, *mdx*, and MTBD/*mdx* mice. A simple linear regression analysis was performed on $\log_{10}$-transformed JP-1 abundance and post:pre-scruff activity ratios to fit a line with equation ($y = -1.541*x + 2.431$) with $R = -0.736$, $R^2 = 0.542$, and a slope that was statistically significantly non-zero ($p = 0.0018$) by an F-test ($F = 15.37$; DFn=1; DFd=13). Box plots depict minimum, Q1, median, Q3, and maximum values from $n = 5$ mice/group. Comparisons between groups were made using two-way ANOVA with Tukey's multiple comparisons test (*$p < 0.05$; **$p < 0.01$; ***$p < 0.001$; ****$p < 0.0001$).

including DMD. Our results point to an exciting myokine candidate that may be implicated in the progression of dystrophinopathy and suggest that monitoring protein post-translational modifications may be an avenue for future investigation in probing dynamic changes that provoke the *mdx* stress response.

An unexpected result of our ECF proteomics investigation was the elevated abundance of several contractile proteins in *mdx* SkM ECF following scruff stress. Scruff handling represents a relatively mild physiological perturbation that is unlikely to cause mechanical injury to the animal's hindlimb muscle compartment, and the post-scruff hypoactivity observed in *mdx* mice suggests there is limited SkM contractile activity following scruff stress. Corroborating the lack of contractile injury is data demonstrating that SkM-type creatine kinase (CK-MM) levels were reduced, rather than elevated, in *mdx* bulk SkM or ECF, independent of scruff stress (main effect

p-value<0.0001). Nonetheless, contractile fiber-associated proteins demonstrated elevated *mdx* post-scruff ECF abundance, including JP-1 (interaction p-value<0.0001), JP-2 (interaction p-value<0.0001), myomesin-1 (interaction p-value=0.0002), myomesin-2 (interaction p-value<0.0001), and tropomyosin alpha-1 chain (interaction p-value=0.002). Meanwhile, JP-1, JP-2, and tropomyosin alpha-1 chain did not show altered abundance in bulk SkM between genotype or treatment condition, while myomesin-1 and myomesin-2 each demonstrated a mild but significant reduction in *mdx* bulk SkM, independent of scruff (genotype main effect p-value<0.05).

Hallmarks of *mdx* pathology, including muscle force production deficits, basal MT lattice organization, post-exercise inactivity, and stress-induced pathology, are rescued in the MTBD/*mdx* model, in spite of the loss of a functional dystrophin MT binding domain.[8,10] Despite a near-complete rescue of *mdx* pathology, MTBD/*mdx* mice do mimic the susceptibility of transgenic *mdx* mice expressing miniaturized dystrophin constructs to transverse MT loss following eccentric contraction in SkM,[54] a finding that is not readily explained by MT-related protein expression changes between MTBD/*mdx* SkM and transgenic *mdx* lines that do rescue ECC-induced MT disorganization.[54] As a corollary to our investigation of the *mdx* SkM secretome, we also sought to identify proteins in the basal QM proteome with compensatory or intermediate expression in MTBD/*mdx* mice compared to WT and *mdx* mice that may explain MTBD/*mdx* MT disorganization. Our data reinforce the broad molecular and phenotypic rescue in MTBD/*mdx* SkM and demonstrate that basal and post-scruff *mdx* SkM proteomic alterations are largely restored to WT status in MTBD/*mdx* SkM. Our finding that HSPB1 levels were reduced in MTBD/*mdx* SkM (main effect p-value = 0.004) aligned with our lab's previous MTBD/*mdx* SkM proteomics data[54] and led us to identify filamin-C (main effect p-value = 0.008) as an additional protein commonly reduced in MTBD/*mdx* SkM compared to MT-rescued control groups between our two proteomics studies. While filamin-C interacts with the sarcoglycan complex,[55] and β-sarcoglycan-null skeletal muscle presents with a disorganized subsarcolemmal MT lattice in the presence of dystrophin,[10] it is not immediately clear how the absence of filamin-C may be contributing to MT instability in dystrophic muscle. Thus, the few proteomic differences between WT and MTBD/*mdx* QM suggest that ECC-induced MT disorganization in MTBD/*mdx* mice is likely due to altered protein post-translation modifications and/or enzyme activities rather than alterations in protein expression.

Among MTBD/*mdx* QM proteins with altered expression compared to WT, we identified PrxII, HSPB1, ADP-ribosylhydrolase like 1 (*Adprhl1*), Rho GDP-dissociation inhibitor 2 (*Arhgdib*), tropomyosin 3, gamma (*Tpm3*), and sarco/endoplasmic reticulum Ca^{2+}-ATPase 2 (SERCA2; *Atp2a2*). Our lab previously demonstrated that SkM PrxII expression is dispensable for MT lattice organization,[54] suggesting that the lack of PrxII rescue in MTBD/*mdx* SkM is unlikely to explain ECC-mediated loss of transverse MTs in MTBD/*mdx* mice. Tropomyosin 3 and SERCA2 regulate actin filament binding and Ca^{2+} dynamics during muscle contraction, respectively. Tropomyosin 3 levels were mildly but not significantly reduced in *mdx* and MTBD/*mdx* QM compared to WT (main effect p-value = 0.06), while SERCA2 levels were significantly reduced in MTBD/*mdx* QM compared to WT and *mdx* (main effect p-value = 0.01). Reduced tropomyosin 3 and SERCA2 expression in MTBD/*mdx* SkM may lead to altered excitation-contraction coupling; however, MTBD/*mdx* mice have fully rescued muscle function and do not display eccentric contraction-induced force drop compared to *mdx* mice.[10] ADP-ribosylhydrolase like 1 is a pseudoenzyme reported to be exclusively expressed in the heart for the regulation of actin cytoskeletal dynamics and Z-disc formation.[56] However, our proteomics data suggests that ADP-ribosylhydrolase like 1 is found in SkM and is reduced in MTBD/*mdx* SkM compared to WT and *mdx* (main effect p-value = 0.007), which may open the door to novel cytoskeletal and MT regulatory functions for ADP-ribosylhydrolase like 1 in SkM.

Additionally, we investigated compensatory or intermediate expression changes in MTBD/*mdx* ECF after scruff exposure that could rule out previously identified pathology-associated *mdx* proteomic alterations as contributing to *mdx* stress vulnerability. Following two-way ANOVA analysis, most of the MTBD/*mdx* DEPs identified by two-group comparisons were shown to demonstrate similar protein expression levels to WT mice, as exemplified by adiponectin and GSTM1.

Interestingly, adiponectin was shown to be elevated in *mdx* QM and depleted in *mdx* ECF, which to our knowledge has not been reported previously and suggests that reduced adiponectin observed in *mdx* and DMD biofluids[57,58] may be due to impaired adiponectin secretion from dystrophin-deficient SkM. The last few years have shown an increased investment in the development of adiponectin-agonist therapies to treat the secondary pathological manifestations of dystrophinopathy in SkM, cardiac muscle, smooth muscle, and the brain[59–65]. Adiponectin secretion is regulated in part by PTMs of its high molecular weight oligomeric form to improve insulin sensitivity, glucose uptake, respiratory capacity, and anti-inflammatory macrophage phenotype switching.[59,66] Recent work has highlighted impaired adiponectin secretion as a contributor to gut dysbiosis in *mdx* mice.[67] An improved mechanistic understanding of possible impairments in the adiponectin secretory pathway within *mdx* SkM will be important for the development of targeted therapies with high efficacy in improving DMD metabolic dysfunction along with muscle inflammation and fibrosis. Dystrophin repletion in MTBD/*mdx*

SkM restores ECF adiponectin levels, exemplifying the multitude of proteomic alterations in *mdx* SkM and circulation that are rescued to WT-like status in MTBD/*mdx* mice.

Our *mdx* ECF and QM proteomics data supports existing literature demonstrating dysregulated glutathione (GSH) and oxidative stress-handling pathways in *mdx* mice and DMD patients[68–70]. Glutathione S-transferases (GSTs) are detoxification enzymes that bind a wide variety of endogenous and exogenous ligands in addition to their catalytic activity in conjugating electrophilic moieties to GSH and performing peroxidase and isomerase functions.[71] Our data demonstrated reduced GSTM1 and GSTM2 levels in *mdx* ECF and QM, while MTBD/*mdx* ECF displayed WT-like GSTM1 and GSTM2 levels in ECF and an additional increment in post-scruff QM levels of these enzymes beyond WT levels after scruff exposure. Glutaredoxin (GRX) enzymes perform cytoprotective functions and protect against protein oxidative stress by catalyzing the reduction of protein mixed disulfides with GSH.[72] GRX-1 levels were significantly reduced in *mdx* ECF compared to WT and MTBD/*mdx* (main effect p-value < 0.0001), while GRX-1 levels were also reduced in *mdx* QM and significantly restored in MTBD/*mdx* QM (main effect p-value = 0.0002). Superoxide dismutase (SOD) and catalase work in tandem to provide cellular antioxidant defense by SOD-mediated superoxide dismutation and catalase-mediated reduction of hydrogen peroxide formed by SOD.[73] We observed reduced SOD2 levels in *mdx* and QM compared to WT and MTBD/*mdx* (main effect p-value < 0.01). Catalase was reduced in MTBD/*mdx* QM compared to WT, with intermediate *mdx* expression (main effect p-value = 0.01); in contrast, ECF catalase levels were significantly reduced in *mdx* mice and increased in MTBD/*mdx* mice following scruff exposure (interaction p-value = 0.006), suggesting a potential compensatory secretion of SkM catalase in MTBD/*mdx* mice as an adaptive stress response. Altogether, our proteomics data supports a model in which SkM dystrophinopathy leads to defects in cellular antioxidant defense machinery and contributes to basally elevated oxidative stress. Additional perturbations in cellular redox homeostasis due to physiological stress exposure are met with poor oxidative stress handling in *mdx* mice and are rescued by SkM dystrophin expression in MTBD/*mdx* mice. Increased post-stress oxidative damage in *mdx* mice may lead to downstream proteomic alterations as well as stress pathology, suggesting that strategies to mitigate oxidative stress may be beneficial in reducing *mdx* stress susceptibility.

Conclusions

In conclusion, we characterized the *mdx* SkM secretome following scruff exposure to identify multiple putative secreted protein candidates whose secretion from SkM is regulated by stress and SkM dystrophinopathy. These protein candidates require further validation with orthogonal biochemical techniques, along with pharmacological and genetic approaches to assess their impact on *mdx* stress physiology. An important strength of our proteomics analysis is the inclusion of a phenotypically rescued group (MTBD/*mdx*) with targeted dystrophin restoration exclusively in the SkM compartment. This group enables us to identify proteomic changes that are specifically related to SkM dystrophinopathy and *mdx* stress pathology, since MTBD/*mdx* mice are also rescued for all *mdx* stress phenotypes.[8,9] Additionally, the data from our current proteomics investigation can be further mined to identify novel secreted proteins that are regulated by dystrophin expression in SkM, with the inclusion of a comparison group that is phenotypically rescued and displays nearly WT-like proteomic expression patterns. Future biomarker identification and pre-clinical investigations of genetic and pharmacological DMD therapies should include MTBD/*mdx* mice or a similar phenotypically and genetically rescued group for comparison of biomarker specificity or treatment efficacy. Additional future investigations will assess the protein, metabolite, and nucleotide contents of SkM extracellular vesicles and exosomes to advance our understanding of the dystrophic SkM secretome during a physiological stress response.

List of abbreviations

DMD	Duchenne muscular dystrophy
SkM	skeletal muscle
ECF	extracellular fluid
WT	wild-type
QM	bulk quadriceps muscle
FSTL1	follistatin-like 1 protein
GO	gene ontology
DEP	differentially expressed protein
PC	principal component
PCA	principal component analysis
FDR	false discovery rate
HSA	human skeletal actin
SLR	spectrin-like repeat
MT	microtubule
WB	western blot
PSM	peptide spectrum match
ELISA	enzyme-linked immunosorbent assay
GSH	glutathione
GST	glutathione S-transferase
GRX	glutaredoxin

Acknowledgements

The authors would like to thank Dr Kurt Prins at the University of Minnesota for his intellectual input and hypothesis generation for data pertaining to skeletal muscle transverse tubule morphology.

Ethical considerations

All animal experiments were approved by the Institutional Animal Care and Use Committee at the University of Minnesota (Protocol #2404-42023A).

Consent to participate

Not applicable

Consent for publication

Not applicable

Author contributions

EJ and JME conceived the study and designed experiments. EJ performed and analyzed proteomics and ELISA experiments. JP performed and EJ analyzed western blot experiments. EJ wrote the manuscript. EJ and JME made manuscript revisions. All authors read and approved the final manuscript.

Funding

This work was supported by the National Institutes of Health (NIH) Minnesota Muscle Training Grant [5T32AR007612-21, 5T32AR007612-22] to EJ, the NIH Functional Proteomics of Aging Training Grant [5T32AG029796-13, 5T32AG029796-14] to EJ, and by NIH grants [5R01AR042423-27] and [5R01AR049899-18] to JME. The Orbitrap Eclipse instrumentation platform used in this work was purchased through High-end Instrumentation Grant S10OD028717 from the NIH.

NIH Functional Proteomics of Aging Training Grant, National Institutes of Health (NIH) Minnesota Muscle Training Grant, National Institutes of Health, (grant numbers 5T32AG029796-13, 5T32AG029796-14, 5T32AR007612-21, 5T32AR007612-22, 5R01AR042423-30, 5R01AR049899-21).

Declaration of conflicting interests

The authors declared no potential conflicts of interest with respect to the research, authorship, and/or publication of this article.

Data availability

The datasets supporting the conclusions of this article are included in the published article (Supplementary Data 1 and 2) and are publicly available in the ProteomeXchange Consortium via the Proteomics Identifications Database (PRIDE) repository, project accession PXD054593.[74] R script used to generate plots and filter data is publicly available at: https://github.com/joh18358/Stress-myokines-proteomics-analysis.

Supplemental material

Supplemental material for this article is available online.

References

1. Duan D, Goemans N, Takeda S, et al. Duchenne muscular dystrophy. *Nat Rev Dis Prim* 2021; 7: 1–19.
2. Thangarajh M, Hendriksen J, McDermott MP, et al. Relationships between DMD mutations and neurodevelopment in dystrophinopathy. *Neurology* 2019; 93: e1597.
3. Poysky J. Behavior patterns in duchenne muscular dystrophy: report on the parent project muscular dystrophy behavior workshop 8–9 of December 2006, Philadelphia, USA. *Neuromuscul Disord* 2007; 17: 986–994.
4. Latimer R, Street N, Conway KC, et al. Secondary conditions among males with Duchenne or Becker muscular dystrophy. *J Child Neurol* 2017; 32: 663–670.
5. Maresh K, Papageorgiou A, Ridout D, et al. Startle responses in Duchenne muscular dystrophy: a novel biomarker of brain dystrophin deficiency. *Brain* 2023; 146: 252–265.
6. Strakova J, Kamdar F, Kulhanek D, et al. Integrative effects of dystrophin loss on metabolic function of the mdx mouse. *Sci Rep* 2018; 8: 1–10.
7. Davidson ZE and Truby H. A review of nutrition in duchenne muscular dystrophy. *J Hum Nutr Diet* 2009; 22: 383–393.
8. Razzoli M, Lindsay A, Law M, et al. Social stress is lethal in the mdx model of Duchenne muscular dystrophy. *EBioMedicine* 2020; 55: 1–11.
9. Johnson EE, Southern WM, Doud B, et al. Retention of stress susceptibility in the mdx mouse model of duchenne muscular dystrophy after PGC-1α overexpression or ablation of IDO1 or CD38. *Hum Mol Genet* 2024; 26: 312–318.
10. Belanto JJ, Olthoff JT, Mader TL, et al. Independent variability of microtubule perturbations associated with dystrophinopathy. *Hum Mol Genet* 2016; 25: 4951–4961.
11. Wolfe RR. The underappreciated role of muscle in health and disease. *Am J Clin Nutr* 2006; 84: 475–482.
12. Florin A, Lambert C, Sanchez C, et al. The secretome of skeletal muscle cells: a systematic review. *Osteoarthr Cartil Open* 2020; 2: 1–21.
13. Lecompte S, Abou-Samra M, Boursereau R, et al. Skeletal muscle secretome in duchenne muscular dystrophy: a pivotal anti-inflammatory role of adiponectin. *Cell Mol Life Sci* 2017; 74: 2487.
14. Rai M, Demontis F and Mem A. Muscle-to-Brain signaling via myokines and myometabolites. *Brain Plast* 2022; 8: 43–63.
15. Severinsen MCK and Pedersen BK. Muscle–organ crosstalk: the emerging roles of myokines. *Endocr Rev* 2020; 41: 94.
16. Hortin GL, Sviridov D and Anderson NL. High-Abundance polypeptides of the human plasma proteome comprising the top 4 logs of polypeptide abundance. *Clin Chem* 2008; 54: 1608–1616.
17. Mittenbühler MJ, Jedrychowski MP, Van Vranken JG, et al. Isolation of extracellular fluids reveals novel secreted bioactive proteins from muscle and fat tissues. *Cell Metab* 2023; 35: 535–549.e7.
18. Yakubovich EI, Polischouk AG and Evtushenko VI. Principles and problems of exosome isolation from biological fluids. *Biochem (Mosc) Suppl Ser A Membr Cell Biol* 2022; 16: 115.

19. Allelein S, Medina-Perez P, Lopes ALH, et al. Potential and challenges of specifically isolating extracellular vesicles from heterogeneous populations. *Sci Reports* 2021; 11: 1–12.
20. Reddy A, Bozi LHM, Yaghi OK, et al. pH-gated succinate secretion regulates muscle remodeling in response to exercise. *Cell* 2020; 183: 62–75.
21. Görgens SW, Raschke S, Holven KB, et al. Regulation of follistatin-like protein 1 expression and secretion in primary human skeletal muscle cells. *Arch Physiol Biochem* 2013; 119: 75–80.
22. Mattiotti A, Prakash S, Barnett P, et al. Follistatin-like 1 in development and human diseases. *Cell Mol Life Sci* 2018; 75: 2339–2354.
23. Xiao X, Zhang H, Ning W, et al. Knockdown of FSTL1 inhibits microglia activation and alleviates depressive-like symptoms through modulating TLR4/MyD88/NF-κB pathway in CUMS mice. *Exp Neurol* 2022; 353: 114060.
24. Chaanine AH, Higgins L, Markowski T, et al. Multi-omics approach profiling metabolic remodeling in early systolic dysfunction and in overt systolic heart failure. *Int J Mol Sci* 2021; 23: 1–31. DOI: 10.3390/ijms23010235.
25. Rappsilber J, Ishihama Y and Mann M. Stop and go extraction tips for matrix-assisted laser desorption/ionization, nanoelectrospray, and LC/MS sample pretreatment in proteomics. *Anal Chem* 2003; 75: 663–670.
26. Panuwet P, Hunter RE, Souza D, et al. Biological matrix effects in quantitative tandem mass spectrometry-based analytical methods: advancing biomonitoring. *Crit Rev Anal Chem / CRC* 2016; 46: 93.
27. Eden E, Navon R, Steinfeld I, et al. GOrilla: A tool for discovery and visualization of enriched GO terms in ranked gene lists. *BMC Bioinform* 2009; 10: –7.
28. Raudvere U, Kolberg L, Kuzmin I, et al. G:profiler: a web server for functional enrichment analysis and conversions of gene lists (2019 update). *Nucleic Acids Res* 2019; 47: W191–W198.
29. Wei Q, Khan IK, Ding Z, et al. NaviGO: interactive tool for visualization and functional similarity and coherence analysis with Gene Ontology. *BMC Bioinform* 2017; 18: 1–13.
30. Watson J, Smith M, Francavilla C, et al. SubcellulaRVis: a web-based tool to simplify and visualise subcellular compartment enrichment. *Nucleic Acids Res* 2022; 50: W718–W725.
31. Bateman A, Martin MJ, Orchard S, et al. Uniprot: the universal protein knowledgebase in 2023. *Nucleic Acids Res* 2023; 51: D523–D531.
32. Day NJ, Zhang T, Gaffrey MJ, et al. A deep redox proteome profiling workflow and its application to skeletal muscle of a duchenne muscular dystrophy model. *Free Radic Biol Med* 2022; 193: 373–384.
33. Roberts TC, Johansson HJ, McClorey G, et al. Multi-level omics analysis in a murine model of Dystrophin loss and therapeutic restoration. *Hum Mol Genet* 2015; 24: 6756–6768.
34. Olthoff JT, Lindsay A, Abo-Zahrah R, et al. Loss of peroxiredoxin-2 exacerbates eccentric contraction-induced force loss in dystrophin-deficient muscle. *Nat Commun* 2018; 9: 1–14. DOI: 10.1038/s41467-018-07639-3.
35. Fang D, Shi X, Lu T, et al. The glycoprotein follistatin-like 1 promotes brown adipose thermogenesis. *Metabolism* 2019; 98: 16–26.
36. Cynthia Martin F, Hiller M, Spitali P, et al. Fibronectin is a serum biomarker for Duchenne muscular dystrophy. *Proteomics Clin Appl* 2014; 8: 269–278.
37. Florio F, Vencato S, Papa FT, et al. Combinatorial activation of the WNT-dependent fibrogenic program by distinct complement subunits in dystrophic muscle. *EMBO Mol Med* 2023; 15: 1–20. DOI: 10.15252/emmm.202317405.
38. Signorelli M, Ayoglu B, Johansson C, et al. Longitudinal serum biomarker screening identifies malate dehydrogenase 2 as candidate prognostic biomarker for duchenne muscular dystrophy. *J Cachexia Sarcopenia Muscle* 2020; 11: 05.
39. Rosenberg AS, Puig M, Nagaraju K, et al. Immune-mediated pathology in Duchenne muscular dystrophy. *Sci Transl Med* 2015; 7: 1–12. DOI: 10.1126/scitranslmed.aaa7322.
40. Capitanio D, Moriggi M, Torretta E, et al. Comparative proteomic analyses of duchenne muscular dystrophy and becker muscular dystrophy muscles: changes contributing to preserve muscle function in becker muscular dystrophy patients. *J Cachexia Sarcopenia Muscle* 2020; 11: 547–563.
41. Xu H, Cai X, Xu K, et al. The metabolomic plasma profile of patients with Duchenne muscular dystrophy: providing new evidence for its pathogenesis. *Orphanet J Rare Dis* 2023; 18: 1–11.
42. Amor F, Vu Hong A, Corre G, et al. Cholesterol metabolism is a potential therapeutic target in Duchenne muscular dystrophy. *J Cachexia Sarcopenia Muscle* 2021; 12: 677–693.
43. Duguez S, Duddy W, Johnston H, et al. Dystrophin deficiency leads to disturbance of LAMP1-vesicle-associated protein secretion. *Cell Mol Life Sci* 2013; 70: 2159–2174.
44. Xi Y, Hao M, Liang Q, et al. Dynamic resistance exercise increases skeletal muscle-derived FSTL1 inducing cardiac angiogenesis via DIP2A–Smad2/3 in rats following myocardial infarction. *J Sport Heal Sci* 2021; 10: 94.
45. Inoue K, Fujie S, Horii N, et al. Aerobic exercise training-induced follistatin-like 1 secretion in the skeletal muscle is related to arterial stiffness via arterial NO production in obese rats. *Physiol Rep* 2022; 10: 1–10. DOI: 10.14814/phy2.15300.
46. Xi Y, Hao M and Tian Z. Resistance exercise increases the regulation of skeletal muscle FSTL1 consequently improving cardiac angiogenesis in rats with myocardial infarctions. *J Sci Sport Exerc* 2019; 1: 78–87.
47. Ouchi N, Oshima Y, Ohashi K, et al. Follistatin-like 1, a secreted muscle protein, promotes endothelial cell function and revascularization in ischemic tissue through a nitric-oxide synthase-dependent mechanism. *J Biol Chem* 2008; 283: 32802–32811.
48. Hayakawa S, Ohashi K, Shibata R, et al. Association of circulating follistatin-like 1 levels with inflammatory and oxidative stress

markers in healthy men. *PLoS One* 2016; 11: 1–8. DOI: 10.1371/journal.pone.0153619.
49. Chaly Y, Hostager B, Smith S, et al. Follistatin-like protein 1 and its role in inflammation and inflammatory diseases. *Immunol Res* 2014; 59: 266–272.
50. Zhou S, Qian B, Wang L, et al. Altered bone-regulating myokine expression in skeletal muscle of duchenne muscular dystrophy mouse models. *Muscle and Nerve* 2018; 58: 573–582.
51. Murakami K, Tanaka M, Usui T, et al. Follistatin-related protein/follistatin-like 1 evokes an innate immune response via CD14 and toll-like receptor 4. *FEBS Lett* 2012; 586: 319–324.
52. Li X, Fang Y, Jiang D, et al. Targeting FSTL1 for multiple fibrotic and systemic autoimmune diseases. *Mol Ther* 2021; 29: 347–364.
53. Lindsay A, Holm J, Razzoli M, et al. Some dystrophy phenotypes of dystrophin-deficient mdx mice are exacerbated by mild, repetitive daily stress. *FASEB J* 2021; 35: e21489.
54. Nelson DM, Fasbender EK, Jakubiak MC, et al. Rapid, redox-mediated mechanical susceptibility of the cortical microtubule lattice in skeletal muscle. *Redox Biol* 2020; 37: 101730.
55. Thompson TG, Chan YM, Hack AA, et al. Filamin 2 (Fln2): a muscle-specific sarcoglycan interacting protein. *J Cell Biol* 2000; 148: 15.
56. Smith SJ, Towers N, Saldanha JW, et al. The cardiac-restricted protein ADP-ribosylhydrolase-like 1 is essential for heart chamber outgrowth and acts on muscle actin filament assembly. *Dev Biol* 2016; 416: 373–388.
57. Hathout Y, Marathi RL, Rayavarapu S, et al. Discovery of serum protein biomarkers in the Mdx mouse model and cross-species comparison to Duchenne muscular dystrophy patients. *Hum Mol Genet* 2014; 23: 6458.
58. Abou-Samra M, Lecompte S, Schakman O, et al. Involvement of adiponectin in the pathogenesis of dystrophinopathy. *Skelet Muscle* 2015; 5: 25.
59. Gandhi S, Sweeney G and Perry CGR. Recent advances in Pre-clinical development of adiponectin receptor agonist therapies for duchenne muscular dystrophy. *Biomedicines* 2024; 12: 1407.
60. Abou-Samra M, Dubuisson N, Marino A, et al. Striking cardioprotective effects of an adiponectin receptor agonist in an aged mouse model of Duchenne muscular dystrophy. *Antioxidants (Basel, Switzerland)* 2024; 13: 1–17. DOI: 10.3390/ANTIOX13121551.
61. Bellissimo CA, Gandhi S, Castellani LN, et al. The slow-release adiponectin analog ALY688-SR modifies early-stage disease development in the D2. Mdx mouse model of Duchenne muscular dystrophy. *Am J Physiol Cell Physiol* 2024; 326: C1011–C1026.
62. Bellissimo CA, Castellani LN, Finch MS, et al. Memory impairment in the D2.mdx mouse model of duchenne muscular dystrophy is prevented by the adiponectin receptor agonist ALY688. *Exp Physiol* 2023; 108: 1108–1117.
63. Dubuisson N, Versele R, de Carrizosa D-L, et al. The Adiponectin Receptor Agonist, ALY688: A Promising Therapeutic for Fibrosis in the Dystrophic Muscle. *Cells* 2023; 12. Epub ahead of print 1 August 2023. DOI: 10.3390/CELLS12162101.
64. Abou-Samra M, Selvais CM, Boursereau R, et al. Adiporon, a new therapeutic prospect for Duchenne muscular dystrophy. *J Cachexia Sarcopenia Muscle* 2020; 11: 518–533.
65. Boursereau R, Abou-Samra M, Lecompte S, et al. Downregulation of the NLRP3 inflammasome by adiponectin rescues Duchenne muscular dystrophy. *BMC Biol* 2018; 16: 33.
66. Zelikovich AS, Quattrocelli M, Salamone IM, et al. Moderate exercise improves function and increases adiponectin in the mdx mouse model of muscular dystrophy. *Sci Rep* 2019; 9. Epub ahead of print 1 December 2019. DOI: 10.1038/s41598-019-42203-z.
67. Jollet M, Mariadassou M, Rué O, et al. Insight into the role of gut Microbiota in Duchenne muscular dystrophy: an age-related study in mdx mice. *Am J Pathol* 2024; 194: 264–279.
68. Lindsay A, McCourt PM, Karachunski P, et al. Xanthine oxidase is hyper-active in Duchenne muscular dystrophy. *Free Radic Biol Med* 2018; 129: 364–371.
69. Careccia G, Saclier M, Tirone M, et al. Rebalancing expression of HMGB1 redox isoforms to counteract muscular dystrophy. *Sci Transl Med* 2021; 13: eaay8416.
70. Petrillo S, Piemonte F, Catteruccia M, et al. Glutathione imbalance in blood of patients with Duchenne muscular dystrophy. *Neuromuscul Disord* 2015; 25: S250.
71. Sheehan D, Meade G, Foley VM, et al. Structure, function and evolution of glutathione transferases: implications for classification of non-mammalian members of an ancient enzyme superfamily. *Biochem J* 2001; 360: 1.
72. Reynaert NL, Ckless K, Guala AS, et al. In situ detection of S-glutathionylated proteins following glutaredoxin-1 catalyzed cysteine derivatization. *Biochim Biophys Acta* 2006; 1760: 380–387.
73. Surai PF, Earle-payne K and Kidd MT. Taurine as a natural antioxidant: from direct antioxidant effects to protective action in various toxicological models. *Antioxidants* 2021; 10: 1–37. DOI: 10.3390/ANTIOX10121876.
74. Perez-Riverol Y, Bandla C, Kundu DJ, et al. The PRIDE database at 20 years: 2025 update. *Nucleic Acids Res* 2025; 53: D543–D553.